Modeling, Simulation, and Non-linear Control of a Rotorcraft Multi-Lift System

Yanguo Song
songyanguopsu@gmail.com
Associate Professor
Nanjing University of Aeronautics and Astronautics

and
Visiting Scholar
The Pennsylvania State University

Joseph F. Horn
joehorn@psu.edu
Associate Professor

ZuQun Li
zxl5012@psu.edu
Graduate Research Assistant

Jack W. Langealaan
jlangelaan@engr.psu.edu
Associate Professor

Department of Aerospace Engineering
The Pennsylvania State University
University Park, PA 16802

ABSTRACT

A simulation model of a rotorcraft multi-lift system is developed and implemented in the MATLAB / Simulink environment. The modeling tool is designed to be modular and generic, capable of modeling various configurations of rotorcraft, spreader bars, and external loads. This paper focuses on simulation and control of a formation of four helicopters carrying a single external load. Rather than treating the aircraft and slung load as a single dynamic system, they are treated as separate rigid bodies each with its own independent equations of motion. All objects in the four-helicopter system are coupled exclusively through elastic cable forces that act on each of the bodies. Analytical checks of the model are performed for the trim and stability characteristics of each helicopter, and results show reasonable and expected behavior due to the physical coupling from the cables. A non-linear control scheme is developed that using an aerodynamic inverse approach. The control calculates desired control inputs based on an inversion of the quasi-steady aerodynamics and the desired trajectory of each helicopter. In order to accurately track the commanded trajectory, the control law makes direct use of the measured cable force acting on each helicopter. The controller's performance is demonstrated in non-linear simulation of a four-helicopter multi-lift system and compared to a standard dynamic inversion controller. Simulation results show that the controller should make explicit use of measured cable forces and moments in order to ensure constant formation and safe separation of the helicopters.

INTRODUCTION

Multi-lift system, the capacity of two or more rotorcraft lifting a common external slung load, could greatly enhance the cargo lifting capacity of the fleet, allowing many types of heavy vehicles or cargo to be transported by rotorcraft. However, safety and pilot workload issues have prevented operational implementation of multi-lift systems.

A number of studies have been conducted to provide a better understanding of the dynamics and handling qualities associated with a single helicopter and a slung load [1, 2, 3]. It is known that helicopters with external slung loads operate within a more limited flight envelope, due to various dynamic couplings between the helicopter and the load. Operational limits and guidelines for operation of a single helicopter and an external load are now well defined [4]. The couplings will obviously become more complex in a multi-lift system. Nonetheless, the use of two or more helicopters to carry a single external load has been periodically proposed and the dynamic characteristics have been investigated both for manned [5, 6, 7] and unmanned rotorcraft [8]. Multi-lift suspensions have received limited flight testing, and have been advocated as an alternative method to increase payloads without developing very large expensive rotorcraft. A significant obstacle to further operational development is the complexity of the system dynamics and difficulties in coordinated control along typical maneuvering flight paths.

Development of practical multi-lift systems will require realistic and comprehensive equations of motion for use in theoretical and simulation studies. Researchers have proposed using suspensions consisting of various configurations of cables and spreader bars, and have developed detailed ideas for nonlinear modeling of these dynamics systems [9, 10, 11]. The equations of motion for a general configuration of the multi-lift system were derived using D'Alembert's principle in conjunction with the virtual work principle and generalized coordinates. Because the selection of appropriate generalized coordinates are case specific, it is very difficult to maintain simplicity of the kinematics and equations in the applications.

The nonlinear model of the twin-lift system described in ref. 5 and 6 was reduced to a case involving only two-dimensional lateral/vertical motion of the entire system.

Presented at the AHS 69th Annual Forum, Phoenix, Arizona, May 21–23, 2013.

Also, the non-linear model for the two-dimensional case was linearized in a hovering condition. The resulting linear model was identical to that of Ref. 7. The annotated result of the modeling and verification of a generic slung-load system using a small-scale helicopter was presented in Ref. 12. The model is derived using a redundant coordinate formulation based on Gauss's Principle of Least Constraint using the Udwadia–Kalaba equation and can be used to model all body-to-body slung-load suspension types. It is also shown how the model can be used for multi-lift systems, either with multiple helicopters or multiple loads.

Current literature has shown that conventional fuselage feedback control systems for helicopters with heavy external loads cannot provide adequate stability margins and simultaneously meet the military helicopter handling qualities specification requirement, particularly in the roll axis [13]. Earlier studies had dealt with the dynamic properties of the linearized twin-lift system about steady-state hover conditions. Manual control aspects of a dual-lift configuration about the hover flight condition have been studied in considerable detail in Ref. 14. The pilot opinion of the flying qualities of the twin-lift configuration in a completely manual control mode has not been favorable, which is primarily due to the significant increase in cockpit workload. Since this factor adversely affects the speed of executing various twin-lift tasks, a high degree of stability and command augmentation become essential for a safe and satisfactory operation.

A nonlinear control technique using state feedback with a reduced order model of the twin-lift system was presented in Ref. 15. This study researched the closed loop performance of nonlinear controllers for the two twin-lift configurations. Also, earlier work [7, 16] on dual-lift utilizing linear analysis tools focused on the spreader bar configuration. It was concluded in these studies that a stability and command augmentation system would be necessary for the twin-lift operation in order to alleviate the intensive workload requirements on part of the Slave helicopter. References [17-19] suggested using a state-feedback based nonlinear automatic controller to provide stability augmentation to the system, which will also simplify the piloting of the dual-lift task. The control technique is based on feedback linearization [20] which has several advantages over controller designs based on linearized dynamics.

An impressive amount of work has gone into the study of helicopter slung load systems, and even multi-lift systems. However, existing modeling techniques tend to be constrained to specific configurations, or rely on highly simplified linearized models. Many of the modeling approaches combine helicopter and load dynamics into a unified set of dynamic equations, which are not easily adapted to different configurations. There is a need for generic modeling tools that are simple but incorporate relevant nonlinearities, and can be readily adapted to different configurations. In addition, such tools can make use of modern analysis environments such as MATLAB / SIMULINK.

There is also a need for effective and practical coordinated control concepts. The present work addresses the control and stabilization of each individual helicopter in the formation. Each helicopter is controlled independently using only on-board sensors, including direct measurement of the cable force acting on the helicopter. The helicopters follow synchronized commanded trajectories. The non-linear controller uses an inverse solution to the aircraft equations of motion and aerodynamic model including the measured force and moment generated by the attached cable.

SYSTEM MODELING

A sketch of various multi-lift helicopter configurations is given in Figure 1. There are several operational concepts considered for multi-lift helicopter system, including use of spreader bars and other arrangements to help ensure safe separation of the lifting rotorcraft.

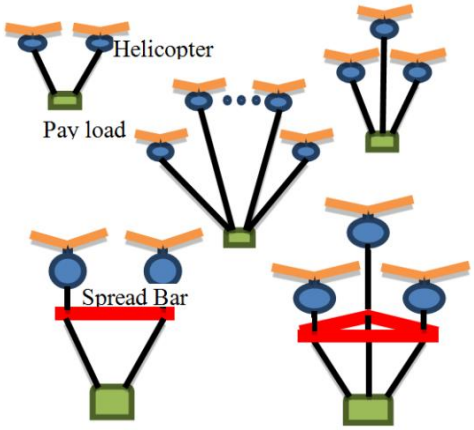

Figure 1. Multi-lift helicopter configurations

For purposes of control design, cable connections can be approximated as elastic, allowing each component to be modeled as a six degree-of-freedom rigid body coupled to each other through cable forces. Cable stretching under tension is treated as a linear spring-damper system. Cable suspension design must avoid an upper bound on frequency set by resonance with the helicopter rotor frequencies or the first fuselage bending modes [4] (around 3-6 Hz for typical helicopters), but should otherwise be as stiff as possible to minimize stretching of the cables. The net result is that natural frequencies of practical suspensions are about 2-2.5Hz. This frequency is sufficiently high to be separated from the frequency range of interest in trajectory control (about 0.5Hz). Thus, for this study, modeling the exact stiffness of the cables was not considered critical. Stiffness was selected such that dynamic modes due to cable stretch were well separated from rigid body dynamics.

The approach taken in this paper is to develop a systematic analytical formulation for general multi-lift slung-load systems, which are readily applied to a variety of

configurations and yield tractable, efficient solutions. In summary, the multi-lift simulation system model will be able to do the following:

- Interface with an existing helicopter simulation math models.
- Accurately model interactions between the helicopter and the slung load.
- Support various flight modes of the helicopter, including hover and cruise flight.
- Support various load types (point mass model or rigid body model).
- Support various load configurations, including any number of helicopters, payloads, spread bars, and other components that can be modeled as rigid bodies connected by elastic cables.

Rather than treating the aircraft and load as a single dynamics system, they are instead treated as separate objects each with its own independent equations of motion, which operate separately, but synchronously [21]. The objects of the multi-lift system are coupled exclusively through the cable forces. To do this, the cable model constantly monitors the spatial relationship between attachment points of loads and aircraft cargo hooks that are connected by the cables. As the relative positions change, a spring/damper model is used to update tensions on each cable, which are then fed into the helicopters' math model and into the load's dynamic model. The method allows the use of existing well-established rotorcraft math models, with minimal modification and without imposing complex constraints.

All multi-lift system configurations shown in Figure 1 can be simplified to several types of dynamic subsystems. These include the helicopter flight dynamics subsystems, cable dynamic subsystems, and spreader bar/payload dynamic subsystems. For this study, a simple nonlinear dynamic model of a utility helicopter was adopted. Spreader bar / payload objects were regarded as rigid bodies and cables as spring-damper elements. These objects are modeled through a library of SIMULINK blocks that can be readily interconnected for different configurations.

Payload/ Spread Bar Rigid Body Model

All spreader bars and payloads are modeled using six degrees of freedom rigid-body mechanics inter connected to other objects or aircraft straight-line links (cables) that can be assumed to be elastic. Given forces and moments applied to the rigid body, the motion can be solved through Newtonian mechanics. Thus, translational and rotational dynamics of the body-fixed frame are modeled with same equations of motion typically used to model aircraft. Spreader bar and payload body forces include cable forces, aerodynamic forces, and hook friction. The following subsections provide some details on these force calculations.

Cable forces are generated from frame to frame by calculating the cable stretching distance between attachment points. The CG location of two connected bodies can be represented by positions vectors: $\begin{bmatrix} x_{rdi,cg} & y_{rdi,cg} & z_{rdi,cg} \end{bmatrix}^T$ and $\begin{bmatrix} x_{rdk,cg} & y_{rdk,cg} & z_{rdk,cg} \end{bmatrix}^T$ in the flat earth reference frame, where subscripts *rdi* and *rdk* indicate the i^{th} and k^{th} rigid bodies. Their attachment point positions are represented by $\begin{bmatrix} x_{rdi,abj} & y_{rdi,abj} & z_{rdi,abj} \end{bmatrix}^T$ and $\begin{bmatrix} x_{rdk,abl} & y_{rdk,abl} & z_{rdk,abl} \end{bmatrix}^T$ in their respective body-fixed frames, where subscript *abj* and *abl* represent the j^{th} and l^{th} attachment point position on the given rigid body *rdi* or *rdk*.

Transformation matrices need to be built, and spatial relationships between the load and aircraft are used to determine the forces on the payloads and the aircraft. A direction cosine matrix is used to translate attachment point position in body frame to the flat earth reference frame. The matrix $R_{rdi,be}$ is the rotation matrix from the NED axes (the flat earth reference frame) to the body axes for rigid body *rdi*. The inverse rotation is simply its transpose.

$$R_{rdi,be} = \begin{bmatrix} \mathrm{c}\theta_{rdi}\,\mathrm{c}\psi_{rdi} & \mathrm{c}\theta_{rdi}\,\mathrm{s}\psi_{rdi} & -\mathrm{s}\theta_{rdi} \\ \mathrm{s}\varphi_{rdi}\,\mathrm{s}\theta_{rdi}\,\mathrm{c}\psi_{rdi} - \mathrm{c}\varphi_{rdi}\,\mathrm{s}\psi_{rdi} & \mathrm{s}\varphi_{rdi}\,\mathrm{s}\theta_{rdi}\,\mathrm{s}\psi_{rdi} + \mathrm{c}\varphi_{rdi}\,\mathrm{c}\psi_{rdi} & \mathrm{s}\varphi_{rdi}\,\mathrm{c}\theta_{rdi} \\ \mathrm{c}\varphi_{rdi}\,\mathrm{s}\theta_{rdi}\,\mathrm{c}\psi_{rdi} + \mathrm{s}\varphi_{rdi}\,\mathrm{s}\psi_{rdi} & \mathrm{c}\varphi_{rdi}\,\mathrm{s}\theta_{rdi}\,\mathrm{s}\psi_{rdi} - \mathrm{s}\varphi_{rdi}\,\mathrm{c}\psi_{rdi} & \mathrm{c}\varphi_{rdi}\,\mathrm{c}\theta_{rdi} \end{bmatrix}$$

$$R_{rdi,eb} = R_{rdi,be}^T \quad (1)$$

The position of attachment point in the NED axis can be shown as,

$$\begin{bmatrix} x_{rdi,anj} \\ y_{rdi,anj} \\ z_{rdi,anj} \end{bmatrix} = \begin{bmatrix} x_{rdi,cg} \\ y_{rdi,cg} \\ z_{rdi,cg} \end{bmatrix} + R_{rdi,eb} \begin{bmatrix} x_{rdi,abj} \\ y_{rdi,abj} \\ z_{rdi,abj} \end{bmatrix} \quad (2)$$

$$\begin{bmatrix} x_{rdk,anl} \\ y_{rdk,anl} \\ z_{rdk,anl} \end{bmatrix} = \begin{bmatrix} x_{rdk,cg} \\ y_{rdk,cg} \\ z_{rdk,cg} \end{bmatrix} + R_{rdi,eb} \begin{bmatrix} x_{rdk,abl} \\ y_{rdk,abl} \\ z_{rdk,abl} \end{bmatrix} \quad (3)$$

where the subscripts *anl* and *anj* represent the locations of attachment points *j* and *l* in the NED frame. Two attachment points in different bodies represent a sling cable, and the distance between two attachment points represents the length of the cable. This distance and the stretch can then be calculated as follows, where the parameter $L_{anj,anl}$ is the unstretched length of the cable.

$$D_{anj,anl} = [(x_{rdi,anj} - x_{rdk,anl})^2 + (y_{rdi,anj} - y_{rdk,anl})^2 + (z_{rdi,anj} - z_{rdk,anl})^2]^{1/2}$$

$$\Delta l_{anj,anl} = D_{anj,anl} - L_{anj,anl} \quad (4)$$

The time rate of change of the stretch (used in the cable damping term) can be calculated by:

$$\Delta\dot{l}_{anj,anl} = [(\dot{x}_{rdi,anj} - \dot{x}_{rdk,anl})(x_{rdi,anj} - x_{rdk,anl}) + (\dot{y}_{rdi,anj} - \dot{y}_{rdk,anl})(y_{rdi,anj} - y_{rdk,anl}) + (\dot{z}_{rdi,anj} - \dot{z}_{rdk,anl})(z_{rdi,anj} - z_{rdk,anl})]\frac{1}{D_{anj,anl}} \quad (5)$$

If $\Delta l_{anj,anl} < 0$ then the cable tension should be $F_{anj,anl} = 0$; else $F_{anj,anl} = K_{anj,anl}\Delta l_{anj,anl} + C_{anj,anl}\Delta\dot{l}_{anj,anl}$. Where parameters $K_{anj,anl}$, and $C_{anj,anl}$ are spring stiffness and damping coefficients respectively. The forces act along the sling cable. The force vector is translated into the NED frame and then the local rigid body frame:

$$\begin{bmatrix} F_{rdi,abj,bx} \\ F_{rdi,abj,by} \\ F_{rdi,abj,bz} \end{bmatrix} = R_{rdi,be}\frac{F_{anj,anl}}{D_{anj,anl}}\left(\begin{bmatrix} x_{rdi,anj} \\ y_{rdi,anj} \\ z_{rdi,anj} \end{bmatrix} - \begin{bmatrix} x_{rdk,anl} \\ y_{rdk,anl} \\ z_{rdk,anl} \end{bmatrix}\right) \quad (6)$$

$$\begin{bmatrix} M_{rdi,abj,bx} \\ M_{rdi,abj,by} \\ M_{rdi,abj,bz} \end{bmatrix} = \begin{bmatrix} 0 & -z_{rdi,abj} & y_{rdi,abj} \\ z_{rdi,abj} & 0 & -x_{rdi,abj} \\ -y_{rdi,abj} & x_{rdi,abj} & 0 \end{bmatrix}\begin{bmatrix} F_{rdi,abj,bx} \\ F_{rdi,abj,by} \\ F_{rdi,abj,bz} \end{bmatrix} \quad (7)$$

Friction at the sling / attach point junctions add a damping effect to load motion. This effect is small compared to the other forces acting on the load and is difficult to quantify from flight test data, due to the predominance of other coupled forces and motions. This damping is implemented as a force proportional to the sling tension and acting to oppose the rotational motion at each attachment point. This effect results in angular damping. The friction moment in the load body axes can then be found using the following equation:

$$\begin{bmatrix} M_{rdi,abj,dampingx} \\ M_{rdi,abj,dampingy} \\ M_{rdi,abj,dampingz} \end{bmatrix} = -K_{rdi,damping}F_{sl,anj,anl}\omega_{rdi,b} \quad (8)$$

where $K_{rdi,damping}$ is the cable damping coefficient and $\omega_{rdi,b}$ is the angular velocity vector of the payload relative to the cable in body coordinates.

Aerodynamic Forces on the Payload and Cable

Unfortunately, there is a lack of aerodynamic data for most externally carried loads with various shapes. At present, however, a simplified aerodynamic model is included that can provide some reasonable steady forces for a wide range of load types – even at the unusual attitudes. This model includes aerodynamic drag forces as described below.

For calculation of body aerodynamic forces, an extension is made to the classical model that characterizes drag of a blunt body in terms of constant flat plate drag areas. Recognizing that the exposed areas are different when subjected to flow from different angles, we define the body with three separate flat plate drag areas $(S_{rdi,top}, S_{rdi,side}, S_{rdi,front})$ and an aerodynamic center as below.

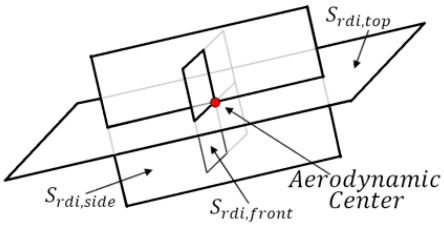

Figure 2. Payload simplified structure model

First, the dynamic pressure is calculated and resolved into its pay load body axes components,

$$\begin{bmatrix} P_{rdi,aerox} \\ P_{rdi,aeroy} \\ P_{rdi,aeroz} \end{bmatrix} = 0.5\rho\begin{bmatrix} u_{rdi,b} \\ v_{rdi,b} \\ w_{rdi,b} \end{bmatrix}V_{rdi} \quad (9)$$

The aerodynamic forces are determined by multiplying the flat plat drag area and drag coefficients for each axis by the component of the dynamic pressure exerted in that axis:

$$\begin{bmatrix} F_{rdi,aerox} \\ F_{rdi,aeroy} \\ F_{rdi,aeroz} \end{bmatrix} = -C_D\begin{bmatrix} P_{rdi,aerox}S_{rdi,front} \\ P_{rdi,aeroy}S_{rdi,side} \\ P_{rdi,aeroz}S_{rdi,top} \end{bmatrix} \quad (10)$$

In the current model, the aerodynamic center remains constant at all attitudes. If it does not coincide with C.G., aerodynamic moments will be generated from these forces.

Sling drag is determined in a similar manner to the body aerodynamic forces. Aerodynamic forces on the cable are given in the following equation.

$$\begin{bmatrix} F_{sli,dragx} \\ F_{sli,dragy} \\ F_{sli,dragz} \end{bmatrix} = -C_{D,sl}\begin{bmatrix} P_{sli,dragx}S_{sli,front} \\ P_{sli,dragy}S_{sli,side} \\ P_{sli,dragz}S_{sli,top} \end{bmatrix} \quad (11)$$

Half of this sling drag is applied to the load attach point, and the other half to the cargo hook.

Resultant of Forces and Moments on the Payload

The cable forces, aerodynamic forces, and damping forces all contribute to the total forces on load body. The total forces can be written:

$$F_{rdi} = \sum_{abj=0}^{abj=abn} F_{rdi,abj,b} + F_{rdi,aero} + 0.5\sum_{sli=0}^{sli=abn} F_{sli,drag} \quad (12)$$

Each of the individual forces discussed above are also fed into the calculation of the total moments about the load's center of gravity:

$$M_{rdi} = \sum_{abj=0}^{abj=abn} M_{rdi,abj,b} + \sum_{abj=0}^{abj=abn} M_{rdi,abj,damping} + M_{rdi,aero} + \sum_{sli=0}^{sli=abn} M_{sli,drag} \quad (13)$$

Load body forces and moments are used to body motion using standard Newtonian equations of motion.

Rotorcraft Model

A simple dynamic model of a utility helicopter (similar to a UH-60 helicopter) has been developed for basic research on multi-lift system dynamics and control. The model was originally developed for educational purposes at Penn State and has been employed in this research with some modifications. Many of the aircraft properties used in the model were taken from the documentation of the GENHEL model of the UH-60A Black Hawk as published in a NASA Contractor report [22]. However, the model is simplified compared to Ref. 22 in that it models only rotor flapping dynamics (no lag dynamics), uses a linear lift aerodynamic model, and makes use of approximate closed form integration of blade loads and total rotor forces. Many aspects of the model were derived from Ref. 23, except that it uses a hinge offset representation of the blade and not a center spring model

The model was developed within the MATLAB software environment and provides a straightforward interface to perform the simulation and data analyses. Scripts can be used to generate large sets of trim solutions, linearized models, and time history simulations. The results can then be managed, analyzed, and displayed using MATLAB tools. The model is implemented in state variable form. The 21-state vector includes 9 rigid body fuselage states (3 velocities and 3 angular rates, and 3 Euler angles), 6 rotor states (flapping dynamics in multi-blade coordinates), 3 inflow states, and 3 engine states. The input vector consists of lateral and longitudinal cyclic pitches, collective pitch, pedal, and the RPM governor input to the engine. For the current analyses, rotor RPM variation is disabled (effectively eliminating three states). The schematic of simulation model is shown in Figure 3.

In order to handle external forces, an interface which can communicate with cable force model is added. The helicopter math model takes the forces for each hook and adds them into the aircraft's total forces and moments.

$$F_{hook} = \sum F_{sl,tension} + 0.5\sum F_{sl,drag} \quad (14)$$

$$M_{hook} = \sum M_{sl,tension} + \sum M_{sl,damping} + \sum M_{sl,drag} \quad (15)$$

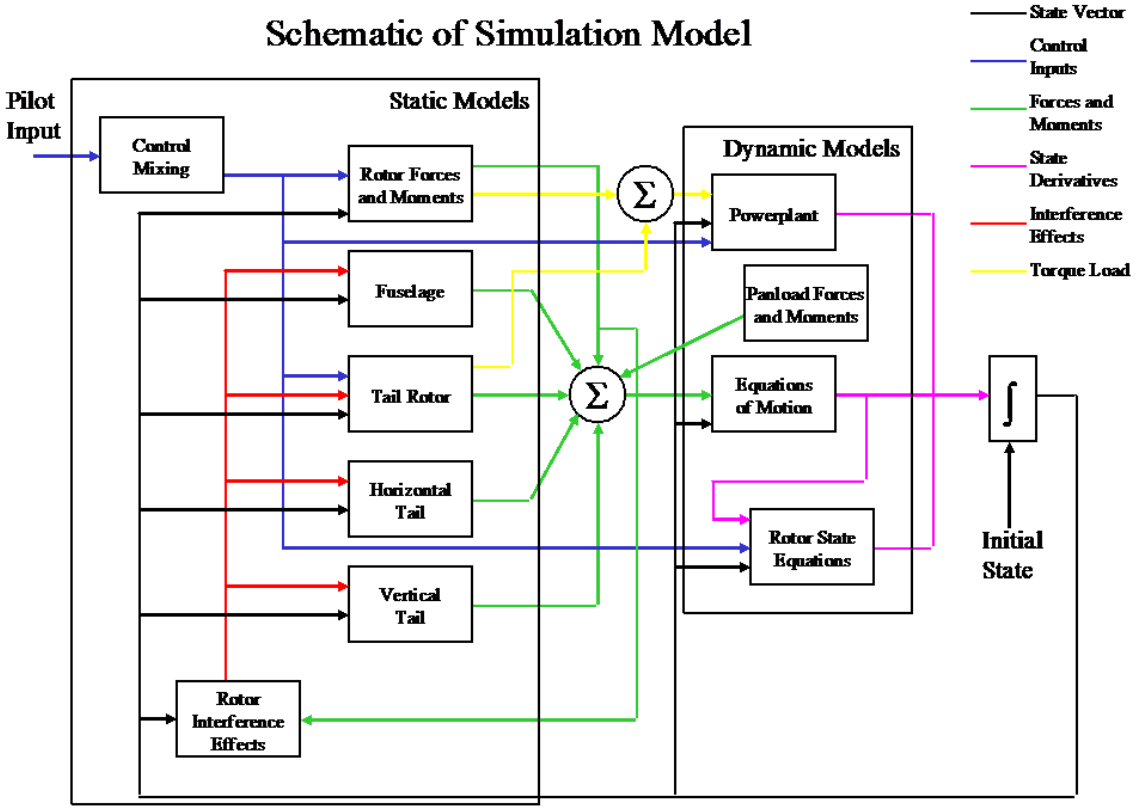

Figure 3. Schematic of the simulation model

MODEL TRIM AND STABILITY

A four-helicopter lift system simulation model was developed in MATLAB/SIMULINK. This configuration is shown in Figure 4. This multi-lift system includes four utility helicopter flight dynamic models (similar to UH-60), four elastics cable models, and one slung load dynamic model. The helicopters in the formation are labeled H1, H2, H3, and H4 as shown in the diagram. Initial inertial coordinates of the aircraft CG are: H1(0,0,0); H2(0, 100, 0), H3 (100,100,0) , and H4 (100,0,0) with units of feet in the NED frame. The hook position on helicopter is (0, 0, 2 ft) in the body frame, the location of attachment points in the slung load body reference frame are (-10,-10,-10), (-10,10,-10), (10,10,-10), and (10,-10,-10). Consistent English engineering unit system is used throughout (lbs, ft, sec). Initial length of the elastic cable is 200 feet and the weight of slung load is 30,000lb. The gross weight of each helicopter is 16,000 lbs.

Figure 5 shows the overall SIMULINK block diagram connecting the four helicopters and the single payload. There are four blocks for each helicopter and one for the payload. Within each block are subsystem blocks modeling the body dynamics, cable forces, controllers and other subsystems. The diagram illustrates the modularity of the simulation environment.

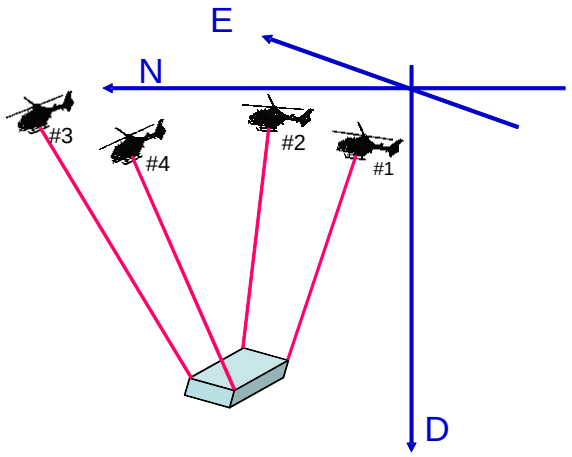

Figure 4. Configuration of four-helicopter lift system

Figures 6 to 9 show the cable forces in the NED frame applied on each helicopter in a trimmed state. In hover, the magnitude of the cable forces are identical for each helicopter but the direction varies due to the helicopter's position in the formation. With increasing forward trim velocity, the cable force magnitude on the rear helicopters (H1 and H2) decreases, and that on the forward helicopters (H3 and H4) increases. This is a result of changing load distribution in the fixed formation as aerodynamic drag forces act on the slung load, as discussed below.

Figures 10-15 show the trim results of all helicopters in the formation (with the formation constrained to a 100 ft square). In order to understand the effects of the slung load, trim results of a single helicopter without a slung load are also shown in the figures. In Figure 10 we can see the helicopters on the left side of the formation (H1 and H4) trim with more of a left bank angle than that seen in normal trim, while those on the right side (H2 and H3) trim with a right bank angle. In Figure 11, the forward helicopters (H3 and H4) have a more nose down pitch attitude, while the aft helicopters (H1 and H2) have a more nose up pitch attitude. Tensions forces on the cable tend to pull the aircraft towards the center of the load, so the helicopters naturally trim so that the next thrust vector pulls away from the load. These results are consistent with this expected behavior. As the aircraft transitions to forward flight, the drag force pushes the slung load aft. With the formation fixed, this requires a larger tension force on the cables connected to the forward aircraft (H3 and H4), which results in higher thrust as reflected in their higher trimmed collective control positions.

Figures 16-19 show the eigenvalues distribution with forward speed from hover to 100 ft/sec forward flight for each helicopter. The eigenvalue distribution of the helicopter without slung load reflects a typical set of rotorcraft modes, including unstable low speed phugoid modes, yaw and heave subsidence modes, and a coupled roll/pitch mode in hover. The modes transition to typical forward flight modes (spiral, roll subsidence, Dutch roll, short period, and phugoid) as speed increases. The modes of each helicopter in the four-helicopter slung load system display clear differences. Dynamic modes are of course coupled across all aircraft and the external loads, but we isolated rigid body modes associated with each aircraft using eigenvectors. Forces and moments generated by the slung load tend to decrease stability of the low speed phugoid and Dutch roll modes. Forces in the horizontal plane also tend to increase coupling between roll and pitch, which degrades stability of the helicopter.

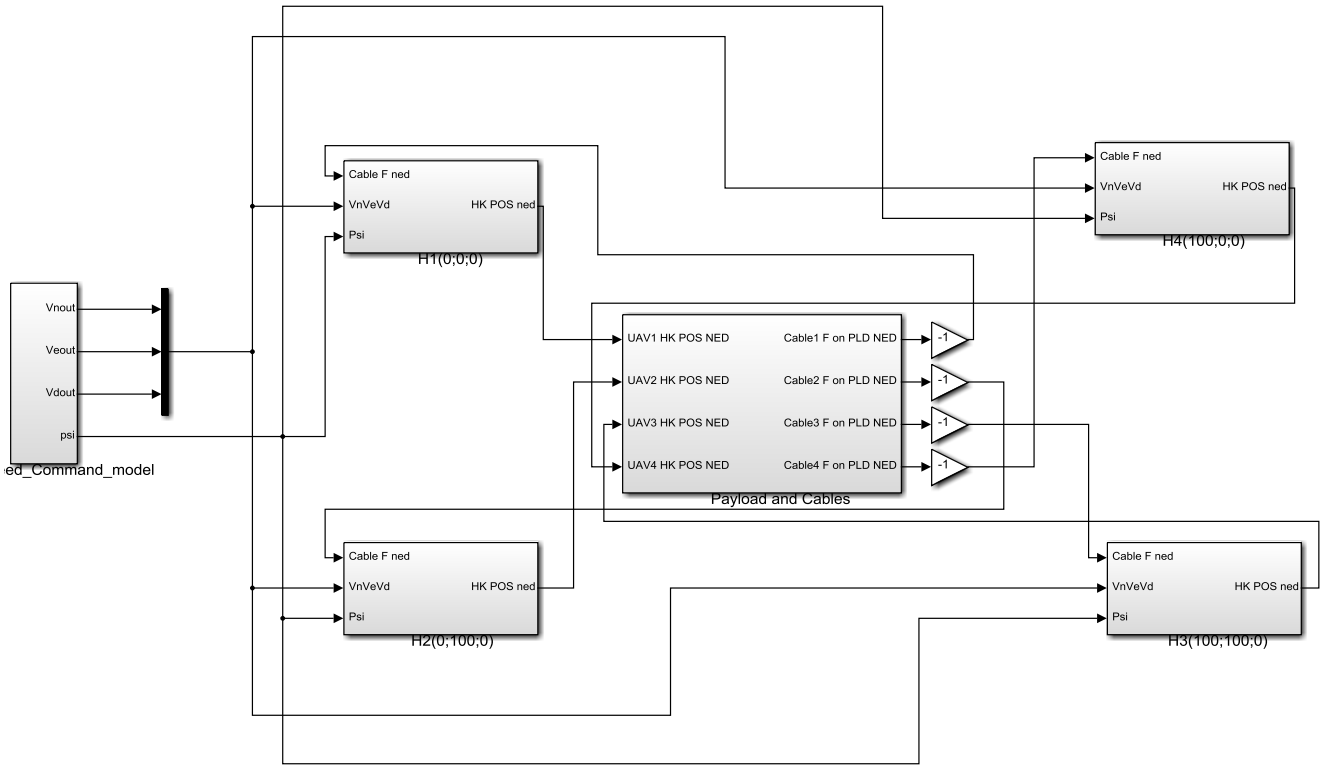

Figure 5. SIMULINK Diagram of four helicopter multi-lift simulation

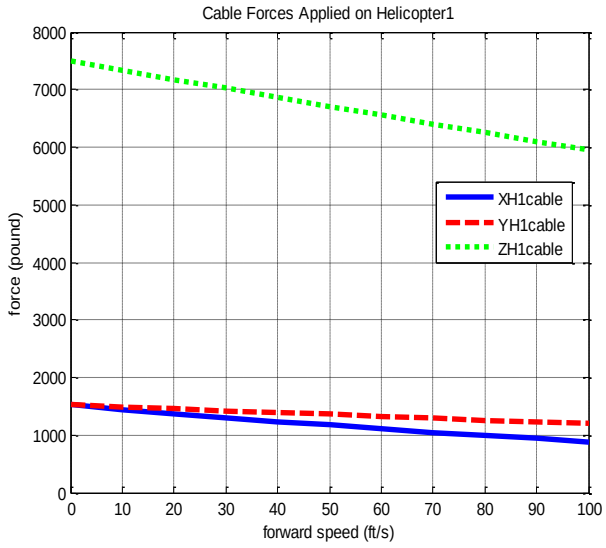

Figure 6. Cable Forces on helicopter 1 in NED frame

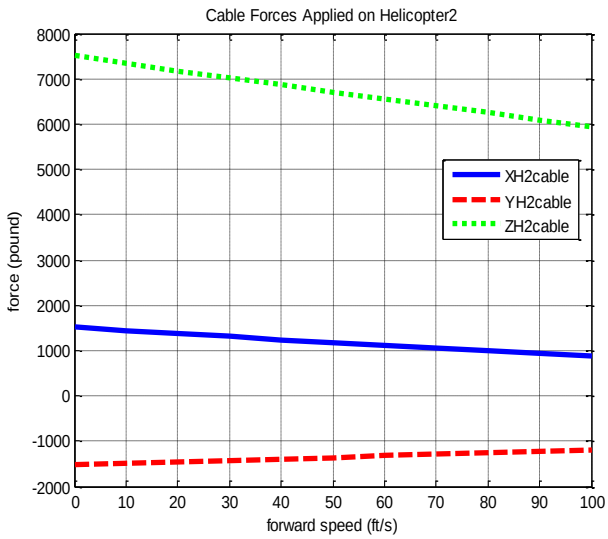

Figure 7. Cable Forces on helicopter 2 in NED frame

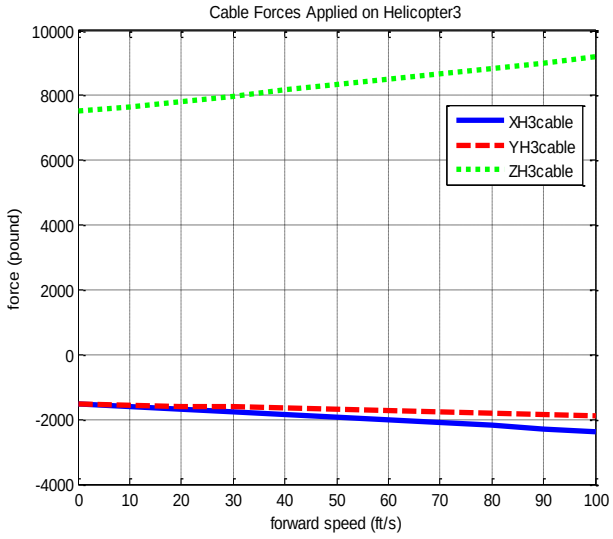

Figure 8. Cable forces on helicopter 3 in NED frame

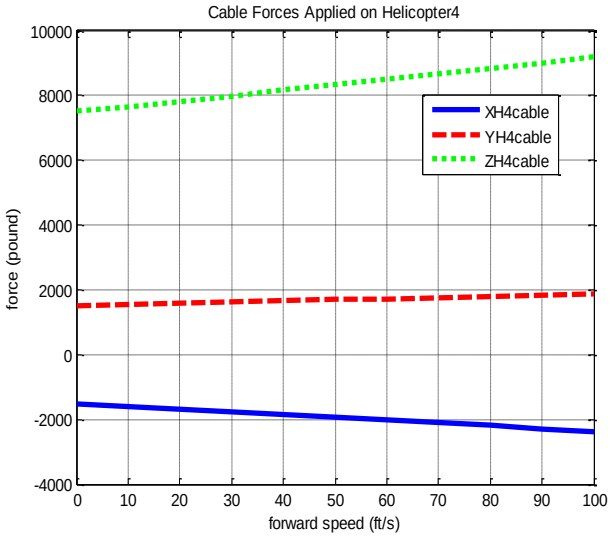

Figure 9. Cable forces on helicopter 4 in NED frame

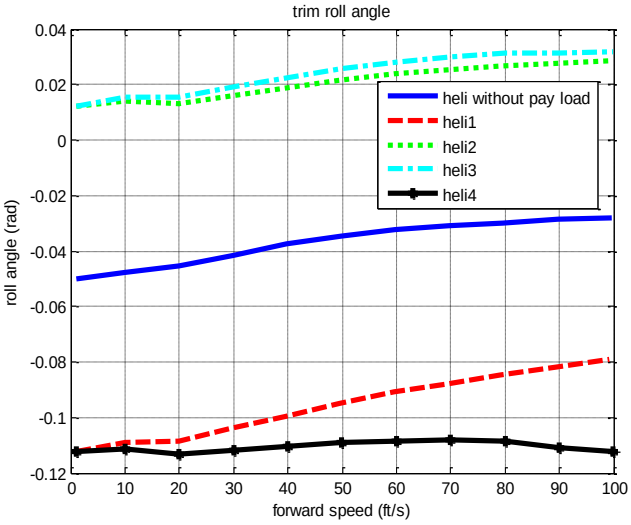

Figure 10. Roll attitude in Trim

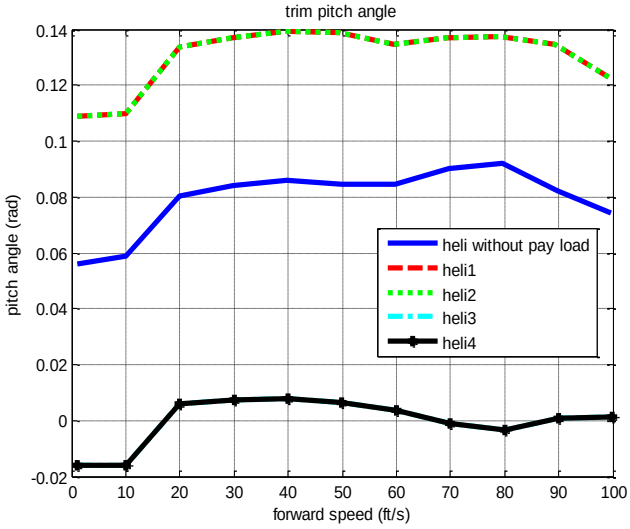

Figure 11. Pitch Attitude in Trim

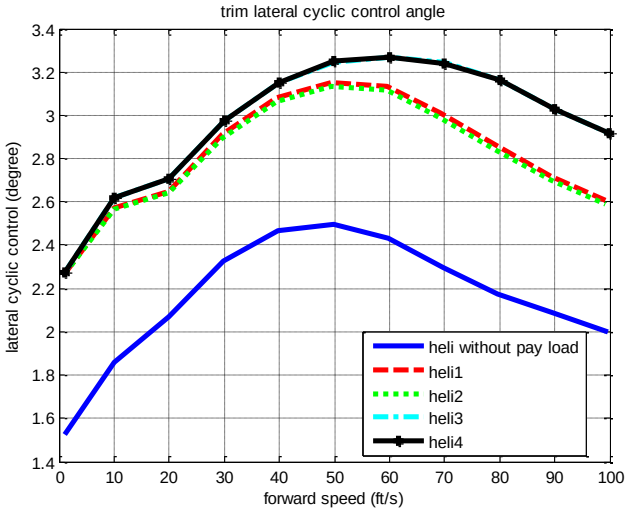

Figure 12. Lateral Cyclic in Trim

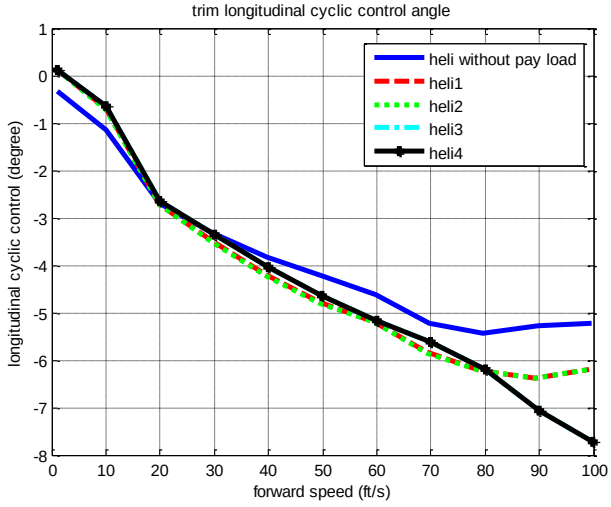

Figure 13. Longitudinal Cyclic in Trim

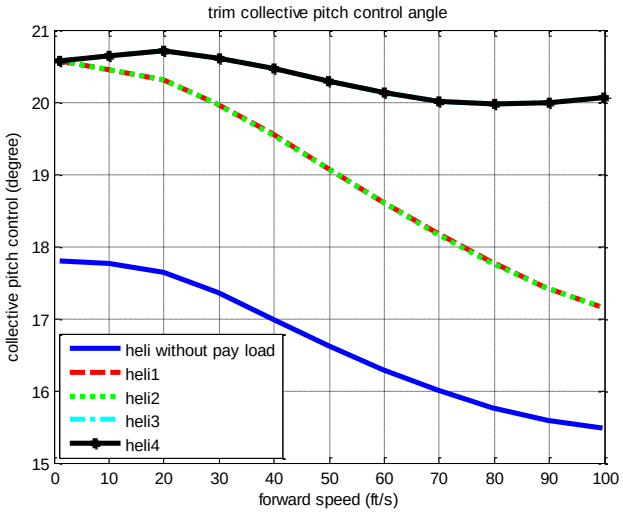

Figure 14. Collective Pitch in Trim

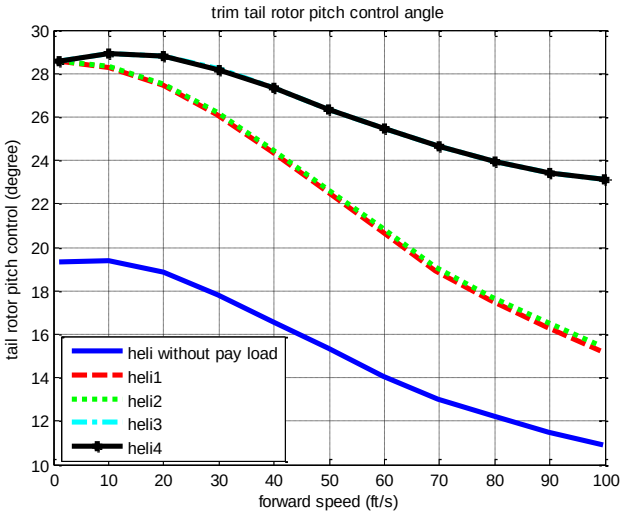

Figure 15. Tail Rotor Collective Pitch in Trim

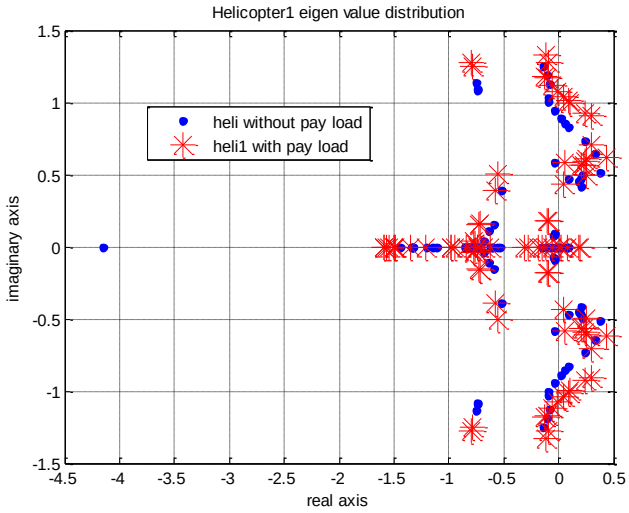

Figure 16. Eigenvalue Distribution of Helicopter 1

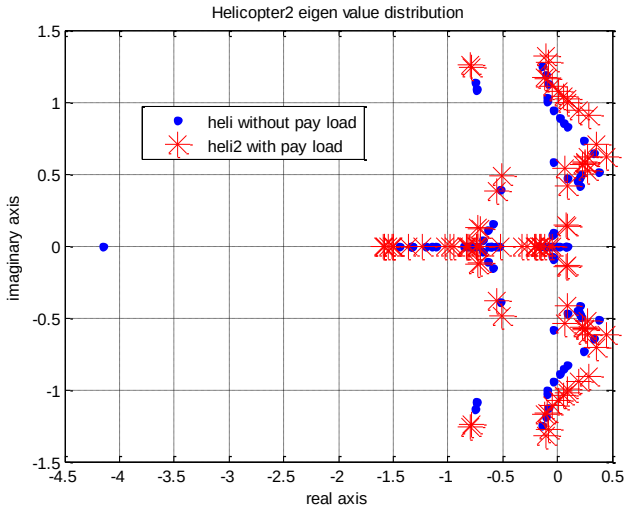

Figure 17. Eigenvalue Distribution of Helicopter 2

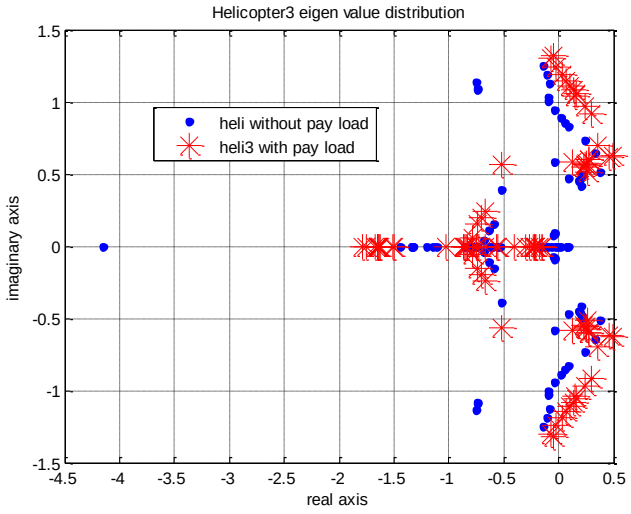

Figure 18. Eigenvalue Distribution of Helicopter 3

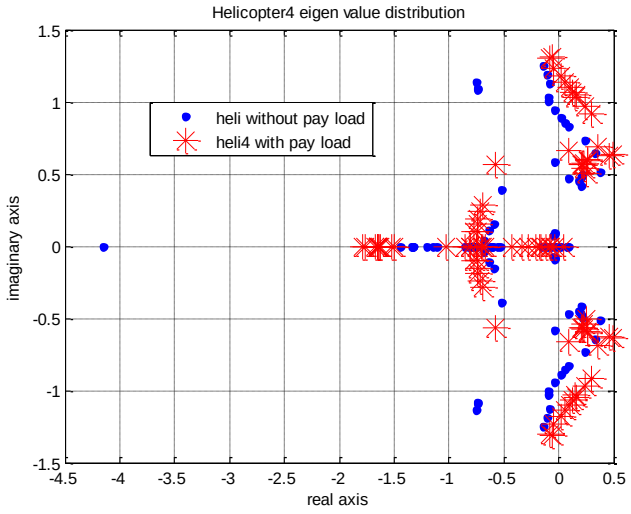

Figure 19. Eigenvalue Distribution of Helicopter 4

NON-LINEAR CONTROL OF MULTI-LIFT SYSTEM

From the eigenvalues of the four-helicopter lift system, we can conclude that:

- Every helicopter has different dynamic modes when operating with the multi-lift payload.
- The stability will change significantly with flight speed and the weight of the payload.
- Every helicopter has different time response under the same input, and it is a challenge to coordinate control.

According to these results, we seek to design a controller for each helicopter that can achieve the following:

- The controller guarantees each helicopter is stable and has similar stability and response characteristics with one another; while, each helicopter has the same control structure to simplify the controller design.
- The dynamic forces and moments generated by the payload have a large influence on individual helicopter's dynamic properties, so these forces and moments should be canceled by the controller.
- The controller should include direct feedback of cable forces to improve its performance and possibly to apply active motion control of the payload to reduce swing during flight.

Nonlinear Controller Using Direct Control Input Calculation through Aerodynamic Inverse

The primary objective of the multi-lift system controllers is to enable the helicopters to carry the load to the desired destination within a specified time-interval. It is vitally important that this maneuver should be carried out while maintaining safe separation between the helicopters and to maintain a reasonable distribution of the load forces. This can be achieved by keeping the lateral, longitudinal, and vertical separations close to some reference values.

Figure 20 illustrates the general concept of the control design. The idea is that, like a human pilot, the controller has some knowledge of the physical system that it is controlling. When a pilot wants the helicopter to follow desired states, they give four control commands (collective pitch, lateral cyclic pitch, longitudinal cyclic pitch, and trail rotor pitch), partly based on an internal model of the aircraft dynamics derived from their flight experience. At the same time, they provide corrective control inputs according to observed deviations between current flight states and the desired states.

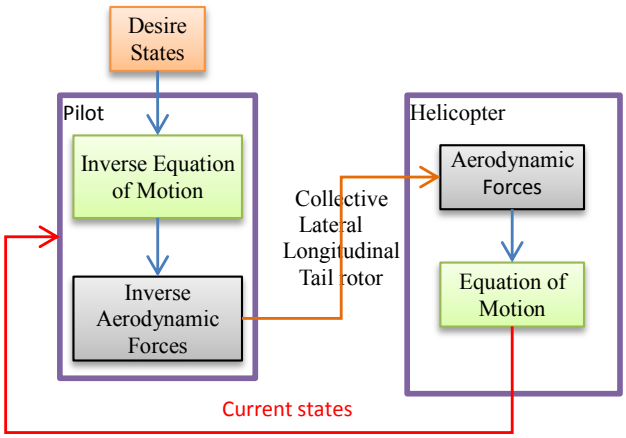

Figure 20 Control input inverse solution

The mathematical model of a helicopter includes two main components: the aerodynamic force module and the equation of motion module. The pilot model can be treated as an intelligent controller with an inverse equation of motion module and an inverse aerodynamic force module. If the inverse modules in the controller are reciprocal to the physical modules then current states will follow desired states. The key aspect of the design is defining the inverse models at an appropriate level of fidelity, so that it can accurately track desired states, and at a reasonable level of simplicity, so that it can be readily implemented.

The helicopter flight rigid body mechanics model can be written as,

$$\begin{aligned} X &= M(\dot{u} - rv + qw) \\ Y &= M(\dot{v} - pw + ru) \\ Z &= M(\dot{w} - qu + pv) \end{aligned} \qquad (16)$$

$$\begin{aligned} L &= I_{xx}\dot{p} - (I_{yy} - I_{zz})qr - I_{xz}(pq + \dot{r}) \\ M &= I_{yy}\dot{q} - (I_{zz} - I_{xx})pr + I_{xz}(p^2 - r^2) \\ N &= I_{zz}\dot{r} - (I_{xx} - I_{yy})pq - I_{xz}(\dot{p} + rq) \end{aligned} \qquad (17)$$

$$\begin{aligned} p &= \dot{\phi} - \dot{\psi}\sin\theta \\ q &= \dot{\theta}\cos\phi + \dot{\psi}\sin\phi\cos\theta \\ r &= -\dot{\theta}\sin\phi + \dot{\psi}\cos\phi\cos\theta \end{aligned} \qquad (18)$$

The right hand sides of Equations (16-18) represent the equation of motion module in Figure 20.

The left hand side of equations (16-18) can be written as,

$$
\begin{aligned}
X &= X_r(x,u_1) + X_{tr}(x,u_2) + X_f(x) + X_h(x) + X_v(x) + X_g(x) + X_c(x)\\
Y &= Y_r(x,u_1) + Y_{tr}(x,u_2) + Y_f(x) + Y_h(x) + Y_v(x) + Y_g(x) + Y_c(x)\\
Z &= Z_r(x,u_1) + Z_{tr}(x,u_2) + Z_f(x) + Z_h(x) + Z_v(x) + Z_g(x) + Z_c(x)\\
L &= L_r(x,u_1) + L_{tr}(x,u_2) + L_f(x) + L_h(x) + L_v(x) + L_c(x)\\
M &= M_r(x,u_1) + M_{tr}(x,u_2) + M_f(x) + M_h(x) + M_v(x) + M_c(x)\\
N &= N_r(x,u_1) + N_{tr}(x,u_2) + N_f(x) + N_h(x) + N_v(x) + N_c(x)
\end{aligned}
\quad (19)
$$

The above equations represent the aerodynamic forces module in Figure 20. Note that the forces and moments are broken into contributions from the various helicopter components, where the subscripts stand for: rotor, *r*; tail rotor, *tr*; fuselage, *f*; horizontal tail plane, *h*; vertical fin, *v*; gravity, *g*; and cable, *c*. Gravity is obviously not an "aerodynamic force", but is included in these terms for simplicity. The force and moment terms are explicit functions of the state vector:

$$x = \left[u, v, w, p, q, r, \varphi, \theta, \psi, \text{ + rotor states}\right]^T$$

and the control vectors:

$$u_1 = [\theta_{1c}, \theta_{1s}, \theta_0]^T, \quad u_2 = [\theta_{0tr}]$$

In equation (19), forces and moments from all components other than the main rotor and tail rotor depend only on states. Of course, if exact aerodynamic interference effects are considered, aerodynamic forces of some components may have a roundabout relationship with control input, but this effect is secondary.

Aerodynamic models are often based on empirical fitting of wind tunnel test data, gathered over a limited range of dynamic pressures and aerodynamic angles and at model scale. Assuming similarity at the test and full-scale flight conditions, the forces at a given airspeed and dynamic pressure can be estimated from the data at the measured conditions through the relationship:

$$F(V_f, \rho_f) = F(V_{test}, \rho_{test})\left(\frac{\rho_f V_f^2 S}{\rho_{test} V_{test}^2 S_{test}}\right) \quad (20)$$

Where the subscript *test* refers to the tunnel test conditions and *S* is a reference area. So forces and moments generated from the fuselage, horizontal stabilizer, vertical fin, and landing gear are all assumed to be known based on measurement of current flight states and atmospheric conditions. In addition, forces and moments generated from the cable are assumed to be measured directly using some kind of external load instrumentation system (e.g. load cells on the cable, cable angle measurement systems, etc …). So, at this point all forces and moments are known except those generated from the main rotor and the tail rotor, which are dependent on control inputs.

If we have the desired commands $[z_r, \phi_r, \theta_r, \psi_r]^T$ and their derivatives, according to equation (18), it is easy to get $[w_r, p_r, q_r, r_r]^T$ and their derivatives. Considering equations (16-19), we have,

$$
\begin{aligned}
&X_r(x,u_1) + X_{tr}(x,u_2) = M(\dot{u} - r_r v + q_r w_r)\\
&-X_f(x) - X_h(x) - X_v(x) - X_g(x) - X_c(x)\\
&Y_r(x,u_1) + Y_{tr}(x,u_2) = M(\dot{v} - p_r w_r + r_r u)\\
&-Y_f(x) - Y_h(x) - Y_v(x) - Y_g(x) - Y_c(x)\\
&Z_r(x,u_1) + Z_{tr}(x,u_2) = M(\dot{w}_r - q_r u + p_r v)\\
&-Z_f(x) - Z_h(x) - Z_v(x) - Z_g(x) - Z_c(x)\\
&(x,u_1) + L_{tr}(x,u_2) = I_{xx}\dot{p}_r - (I_{yy} - I_{zz})q_r r_r - I_{xz}(p_r q_r + \dot{r}_r)\\
&-L_f(x) - L_h(x) - L_v(x) - L_c(x)\\
&M_r(x,u_1) + M_{tr}(x,u_2) = I_{yy}\dot{q}_r - (I_{zz} - I_{xx})p_r r_r + I_{xz}(p_r^2 - r_r^2)\\
&-M_f(x) - M_h(x) - M_v(x) - M_c(x)\\
&N_r(x,u_1) + N_{tr}(x,u_2) = I_{zz}\dot{r}_r - (I_{xx} - I_{yy})p_r q_r - I_{xz}(\dot{p}_r + r_r q_r)\\
&-N_f(x) - N_h(x) - N_v(x) - N_c(x)
\end{aligned}
\quad (21)
$$

The first part of the right hand side of in equation (21) represents the inverse equations of motion module. It is assumed to be known based on a state measurement system. The last part represents forces generated by all components other than the main rotor and tail rotor, which can be estimated through aerodynamic look up tables. Therefore, the right hand side of equations is assumed to be known.

These equations provide the desired forces and moments we want generated from main rotor and tail rotor to realize the desired flight states. We want to find a procedure to solve for control inputs based on equation (21). The process solves for main rotor and tail rotor's collective pitch, main rotor's longitudinal and lateral pitch. Since there are only four primary controls, we cannot enforce all six force and moment constraints. Instead, we will focus on the three moments and the vertical force. There may then be mismatch between the actual *X* and *Y* forces and those required for the desired trajectory. However, these are found to have only a secondary effect on overall vehicle trajectory.

Substitute the vertical force and moment equations (21) into the corresponding equations from the equations of motion module (16, 17), and we can obtain the following:

$$
\begin{aligned}
&M(\dot{w}_r - q_r u + p_r v) = M(\dot{w} - qu + pv)\\
&I_{xx}\dot{p}_r - (I_{yy} - I_{zz})q_r r_r - I_{xz}(p_r q_r + \dot{r}_r) = I_{xx}\dot{p} - (I_{yy} - I_{zz})qr - I_{xz}(pq + \dot{r})\\
&I_{yy}\dot{q}_r - (I_{zz} - I_{xx})p_r r_r + I_{xz}(p_r^2 - r_r^2) = I_{yy}\dot{q} - (I_{zz} - I_{xx})pr + I_{xz}(p^2 - r^2)\\
&I_{zz}\dot{r}_r - (I_{xx} - I_{yy})p_r q_r - I_{xz}(\dot{p}_r + r_r q_r) = I_{zz}\dot{r} - (I_{xx} - I_{yy})pq - I_{xz}(\dot{p} + rq)
\end{aligned}
\quad (22)
$$

Then, when we put the inverse model in series with the aircraft we have

$$\nu \triangleq \begin{bmatrix} \ddot{z}_r \\ \dot{p}_r \\ \dot{q}_r \\ \dot{r}_r \end{bmatrix} = \begin{bmatrix} \ddot{z}_r \\ \ddot{\varphi}_r \\ \ddot{\theta}_r \\ \ddot{\psi}_r \end{bmatrix} \Rightarrow \begin{bmatrix} \ddot{z} \\ \ddot{\varphi} \\ \ddot{\theta} \\ \ddot{\psi} \end{bmatrix} = \nu \quad (23)$$

Here we have defined the pseudo-control vector, $\nu = [\ddot{z}_r, \ddot{\varphi}_r, \ddot{\theta}_r, \ddot{\psi}_r]^T$. The complex dynamic system has been transformed into a linear system. In fact, it is a system of decoupled integrators. We can now design a controller for this system using any linear controller design method. The concept is similar to feedback linearization schemes used in dynamic inversion and other methods. For our application, the most meaningful advantage is that any measured external forces and moments applied on the helicopter can directly feed into the nonlinear controllers of each helicopter – specifically the cable forces and moments. This will allow each helicopter to have nearly identical stability and response characteristics when operating in the multi-lift system.

The next step is to solve helicopter desired control inputs based on known values of the right hand side of equation (21) using a simplified model of the helicopter aerodynamics. The following subsection will present the solution of helicopter control inputs.

Control Input Solution

The method of direct control input calculation using aerodynamic inverse (or just "aerodynamic inverse") is now presented. The method focuses on the key aerodynamic features, which most significantly affect the helicopter's dynamic response. The method is based primarily on simplified versions of the models presented in Ref. 23.

Main rotor forces in the body axis can be written as:

$$\begin{bmatrix} X_r \\ Y_r \\ Z_r \end{bmatrix} = T_{bh} \cdot T_{hw} \begin{bmatrix} CX_{hw}(\rho\Omega^2 R^4) \\ CY_{hw}(\rho\Omega^2 R^4) \\ -CT\,(\rho\Omega^2 R^4) \end{bmatrix} \quad (24)$$

This includes the rotation matrices that transform force from hub axis to body axis (by a rotation by the shaft tilt, γ) and from the hub/wind system to the hub system, as rotated about the shaft by the rotor sideslip angle, ψ_w.

$$\cos\psi_w = u_h \Big/ \sqrt{u_h^2 + v_h^2} \quad (25)$$

$$\sin\psi_w = v_h \Big/ \sqrt{u_h^2 + v_h^2} \quad (26)$$

$$\begin{bmatrix} u_h \\ v_h \\ w_h \end{bmatrix} = T_{hb} \begin{bmatrix} u - qh_r \\ v + ph_r + rx_r \\ w - qx_r \end{bmatrix} \quad (27)$$

CX_{hw} and CY_{hw} are in-plane force coefficients which result from a combination of physical effects. In general, in-plane forces include two main components, the first harmonics of the product of the lift and flapping, and the first harmonics of the aerodynamic drag forces. At moderate speeds, the lift forces can be assumed dominant, and in-plane hub forces are simply approximated by the tilt of the rotor thrust vector,

$$\begin{bmatrix} CX_{hw} \\ CY_{hw} \end{bmatrix} = \begin{bmatrix} CT \cdot \beta_{1cw} \\ -CT \cdot \beta_{1sw} \end{bmatrix} \quad (28)$$

The rotor forces then can be expressed as

$$\begin{bmatrix} X_r \\ Y_r \\ Z_r \end{bmatrix} = T_{bh} \cdot T_{hw} \begin{bmatrix} CT \cdot \beta_{1cw}(\rho\Omega^2 R^4) \\ -CT \cdot \beta_{1sw}(\rho\Omega^2 R^4) \\ -CT\,(\rho\Omega^2 R^4) \end{bmatrix} \quad (29)$$

The rotor moments can be expressed as

$$\begin{bmatrix} L_r \\ M_r \\ N_r \end{bmatrix} = T_{bh} \cdot \begin{bmatrix} CL_h(\rho\Omega^2 R^5) \\ CM_h(\rho\Omega^2 R^5) \\ CQ\,(\rho\Omega^2 R^5) \end{bmatrix} + \begin{bmatrix} 0 & -h_r & y_r \\ h_r & 0 & x_r \\ -y_r & -x_r & 0 \end{bmatrix} \begin{bmatrix} X_r \\ Y_r \\ Z_r \end{bmatrix} \quad (30)$$

The rotor torque produces a dominant component about the shaft axis, plus smaller components in pitch and roll due to the inclination of the rotor relative to the plane normal to the shaft. The tilt results in components of the torque in the roll and pitch directions. This can be represented using the approximation derived in Ref. 23:

$$\begin{bmatrix} CL_{hQ} \\ CM_{hQ} \end{bmatrix} = \begin{bmatrix} -CQ/2 & 0 \\ 0 & CQ/2 \end{bmatrix} \begin{bmatrix} \beta_{1c} \\ \beta_{1s} \end{bmatrix} = \begin{bmatrix} 0 & -CQ/2 \\ CQ/2 & 0 \end{bmatrix} \begin{bmatrix} \beta_{1s} \\ \beta_{1c} \end{bmatrix}$$
$$= \begin{bmatrix} 0 & -CQ/2 \\ CQ/2 & 0 \end{bmatrix} \overline{T_{hw}} \begin{bmatrix} \beta_{1sw} \\ \beta_{1cw} \end{bmatrix} \quad (31)$$

In this equation the wind-to-hub-wind transformation uses only the first two rows and columns of the rotation matrix.

Roll (L) and pitch (M) hub moments are also generated due to rotor stiffness effects (from hinge offset for example), which can be represented as simple linear functions of the flapping angles in multiple blade coordinates (MBC):

$$\begin{bmatrix} L_h \\ M_h \end{bmatrix} = -\frac{N_b K_\beta}{2} \begin{bmatrix} \beta_{1s} \\ \beta_{1c} \end{bmatrix} = -\frac{N_b K_\beta}{2} \overline{T_{hw}} \begin{bmatrix} \beta_{1sw} \\ \beta_{1cw} \end{bmatrix} \quad (32)$$

where K_β is an equivalent hub spring parameter. Then main rotor moments then can be written as

$$\begin{bmatrix} L_r \\ M_r \\ N_r \end{bmatrix} = T_{bh} \cdot \left[\left(\begin{bmatrix} 0 & -CQ/2 \\ CQ/2 & 0 \end{bmatrix} - \frac{N_b K_\beta}{2} \right) \overline{T_{hw}} \begin{bmatrix} \beta_{1sw} \\ \beta_{1cw} \end{bmatrix} \right] \\ CQ\ (\rho\Omega^2 R^5) \\ + \begin{bmatrix} 0 & -h_r & y_r \\ h_r & 0 & x_r \\ -y_r & -x_r & 0 \end{bmatrix} \begin{bmatrix} X_r \\ Y_r \\ Z_r \end{bmatrix} \quad (33)$$

Now we examine tail rotor forces. Ignoring tail rotor flapping and in plane forces, we can approximate tail rotor forces and moments in the body axis as:

$$\begin{aligned} X_{tr} &= 0 \\ Y_{tr} &= CT_{tr}\rho\Omega_{tr}^2 R_{tr}^4 \\ Z_{tr} &= 0 \\ L_{tr} &= h_{tr} CT_{tr}\rho\Omega_{tr}^2 R_{tr}^4 \\ M_{tr} &= CQ_{tr}\rho\Omega_{tr}^2 R_{tr}^5 \\ N_{tr} &= -l_{tr} CT_{tr}\rho\Omega_{tr}^2 R_{tr}^4 \end{aligned} \quad (34)$$

Total forces and moments of the main and tail rotor can then be represented by:

$$\begin{bmatrix} X_{r\_tr} \\ Y_{r\_tr} \\ Z_{r\_tr} \end{bmatrix} = T_{bh} \cdot T_{hw} \begin{bmatrix} CT \cdot \beta_{1cw} (\rho\Omega^2 R^4) \\ -CT \cdot \beta_{1sw} (\rho\Omega^2 R^4) \\ -CT\ (\rho\Omega^2 R^4) \end{bmatrix} + \begin{bmatrix} 0 \\ CT_{tr}\rho\Omega_{tr}^2 R_{tr}^4 \\ 0 \end{bmatrix} \quad (35)$$

$$\begin{bmatrix} L_{r\_tr} \\ M_{r\_tr} \\ N_{r\_tr} \end{bmatrix} = T_{bh} \cdot \left[\left(\begin{bmatrix} 0 & -CQ/2 \\ CQ/2 & 0 \end{bmatrix} - \frac{N_b K_\beta}{2} \right) \overline{T_{hw}} \begin{bmatrix} \beta_{1sw} \\ \beta_{1cw} \end{bmatrix} \right] \\ CQ\ (\rho\Omega^2 R^5) \\ + \begin{bmatrix} 0 & -h_r & y_r \\ h_r & 0 & x_r \\ -y_r & -x_r & 0 \end{bmatrix} \begin{bmatrix} X_r \\ Y_r \\ Z_r \end{bmatrix} + \begin{bmatrix} h_{tr} CT_{tr}\rho\Omega_{tr}^2 R_{tr}^4 \\ CQ_{tr}\rho\Omega_{tr}^2 R_{tr}^5 \\ -l_{tr} CT_{tr}\rho\Omega_{tr}^2 R_{tr}^4 \end{bmatrix} \quad (36)$$

In order to meet desired commands $[z_r, \phi_r, \theta_r, \psi_r]^T$, we substitute the desired commands and current flight states into equation (21), calculate aerodynamics of all components other than the main rotor and tail rotor, and then calculate the desired forces and moments of the rotors, $[Z_{r\_tr}, L_{r\_tr}, M_{r\_tr}, N_{r\_tr}]^T$. Based on these conditions, the desired forces $[X_{r\_tr}, Y_{r\_tr}]^T$, can be also be obtained. The *X* and *Y* force constraints cannot be guaranteed in the control solution, but there values can be used as initial value in the following control input solution.

The control inputs do not explicitly appear in the control forces and moment equations of Equation 35 and 36. We must bring in additional expressions for the force and torque coefficients, cyclic flapping, and inflow as described in Ref. 23. However, these various expressions are coupled, and thus we need a logical progression in the control calculation, which will proceed as follows:

1. Calculate vertical force, Z_r, and main rotor thrust coefficient *CT* for the vertical axis constraint.

2. Calculate main rotor inflow using the following:

$$\lambda_0 = \frac{CT}{2\sqrt{\mu^2 + (\lambda_0 - \mu_z)^2}} \\ \mu = V\cos\alpha_d / \Omega R,\ \mu_z = V\sin\alpha_d / \Omega R \quad (37)$$

3. Calculate the main rotor torque coefficient using the following approximate equation from Ref. 23:

$$\frac{2CQ}{\alpha_0 s} = -(\mu_z - \lambda_0)\left(\frac{2CT}{\alpha_0 s}\right) + \mu\left(\frac{2CT\hat{\beta}_{1cw}}{\alpha_0 s}\right) + \frac{\delta}{4\alpha_0}(1 + 3\mu^2) \quad (38)$$

   Now at this point, the longitudinal flapping term is not known. However, we can use the value from the previous time step and if needed iterate this and the following two steps until the values converge.

4. With torque calculated we can derive the main rotor and tail rotor yaw, N_{r_tr}, and then the tail rotor rotor thrust coefficient, CT_{tr}. Tail rotor inflow can be derived using an expression similar to Equation 37. We can then extract tail rotor collective pitch from the following:

$$CT_{tr} = \frac{\alpha_{0tr} s_{tr}}{2}\left[\theta_{0tr}\left(\frac{1}{3} + \frac{\mu_{tr}^2}{2}\right) + \frac{\mu_{ztr} - \lambda_{0tr}}{2} + \frac{1}{4}\left(1 + \mu_{tr}^2\right)\theta_{twtr}\right] \quad (39)$$

5. From the total roll and pitch moment equations, L_{r_tr} and M_{r_tr}, we can now derive the lateral and longitudinal flapping angles in the hub-wind frame, β_{1sw} and β_{1cw}. Since the flapping angle is now known we can iterate back to step 3 if needed.

6. Flapping angles are converted into the hub frame, and then we use the following two expressions to simultaneously solve for the main rotor controls (lateral, longitudinal cyclic and collective pitch):

$$\begin{bmatrix} \beta_{1s} \\ \beta_{1c} \end{bmatrix} = A_{\beta\theta} \begin{bmatrix} \theta_0 \\ \theta_{tw} \\ \theta_{1sw} \\ \theta_{1cw} \end{bmatrix} + A_{\beta\lambda}\left[\mu_z - \lambda_0\right] + A_{\beta\omega} \begin{bmatrix} \bar{p}_{hw} \\ \bar{q}_{hw} \end{bmatrix} \quad (40)$$

$$CT = \frac{\alpha_0 s}{2}\left[\theta_0\left(\frac{1}{3}+\frac{\mu^2}{2}\right)+\frac{\mu_z-\lambda_0}{2}+\frac{1}{4}\left(1+\mu^2\right)\theta_{tw}+\frac{\mu}{2}\left(\theta_{1sw}+\frac{\bar{p}_{hw}}{2}\right)\right] \quad (41)$$

Equation 40 gives the quasi-static flapping response to collective and cyclic pitch inputs as described in reference 23, where the *A* matrices are a function of the airspeed (advance ratio) and θ_{tw} is the blade twist angle (a constant for the rotor system). Coupled with equation 41, this results in 3 independent equations and 3 unknown variables: θ_0, θ_{1cw}, and θ_{1sw}. The lateral cyclic pitch variables are in hub-wind axes and simply need to be transformed back to the hub frame to calculate the cyclic inputs.

It should be noted, that while we have used numerous equations to solve the aerodynamic inverse solution, the model in the controller is quite simple. It is significantly simpler than the simulation model used to demonstrate the controller. For example, unlike the simulation model, the aerodynamic inverse model uses a simple center spring representation of the rotor, has quasi-static flapping and inflow dynamics, and uniform inflow.

Outer Loop Controller Design

The inversion process results in the roll, pitch, yaw, and vertical response of the aircraft acting as a set of decoupled second order integrators. A simple linear system such as this is easily controlled by a set of simple constant gain PID (proportional, integral, and derivative) control laws. This achieved by modifying the pseudo-control vector in equation (23) as follows:

$$v = \begin{bmatrix} \ddot{z}_c + K_{D\dot{z}}(\dot{z}_c - \dot{z}) + K_{Pz}(z_c - z) + K_{Iz}\int(z_c - z)dt \\ \ddot{\phi}_c + K_{D\dot{\phi}}(\dot{\phi}_c - \dot{\phi}) + K_{P\phi}(\phi_c - \phi) + K_{I\phi}\int(\phi_c - \phi)dt \\ \ddot{\theta}_c + K_{D\dot{\theta}}(\dot{\theta}_c - \dot{\theta}) + K_{P\theta}(\theta_c - \theta) + K_{I\theta}\int(\theta_c - \theta)dt \\ \ddot{\psi}_c + K_{D\dot{\psi}}(\dot{\psi}_c - \dot{\psi}) + K_{P\psi}(\psi_c - \psi) + K_{I\psi}\int(\psi_c - \psi)dt \end{bmatrix} \quad (42)$$

K_P, K_D, K_I are individual loop gains that can be designed to meet performance specifications in attitude and altitude control. Outer loop speed and position control laws can then be designed using similar methods; discussion of these is beyond the scope of this paper.

CLOSED-LOOP SIMULATION RESULTS

In order to understand the performance of the proposed control law, two control laws have been analyzed in simulation. One is based on the Aerodynamic Inversion method as discussed in the previous section, and the other controller is based on a classic linear dynamic inversion control as described in Ref. 24 (for brevity details are not included here). The control modes for both controllers are heading holding, ground speed tracking, and altitude hold. Simulation results of the closed-loop helicopter without the slung load are shown in Figures 21 and 22. The trajectory commands were to increase north (forward) speed from hover to 10 ft/s at the initial time, while holding heading and other ground speeds to zero. The simulation results show that both control laws ensure a stable response with reasonable performance. The aerodynamic inverse controller does exhibit more oscillation in the initial transient of the maneuvers, but it also shows lower tracking error to commanded velocities in both the transient response and steady-state.

The aerodynamic inversion and dynamic inversion controllers were applied to each aircraft in the four-helicopter multi-lift system and tested in simulation. In order to guarantee stability of the standard dynamic inverse control law (which does not account for the slung load cable forces), the payload weight was reduced to 3000 lbs for these results. The commanded trajectories use a fixed 100 ft square formation identical to that used in the open-loop trim and stability analyses. The trajectory command is a 10 ft/sec increase in forward speed starting from hover, just as in the single helicopter results of Figures 21 and 22. Sample results are shown in Figures 23-28, including attitudes, position, and control activity. Results are shown only for helicopters H1 and H3, which are located at the back / right, and forward / left positions of the formation respectively.

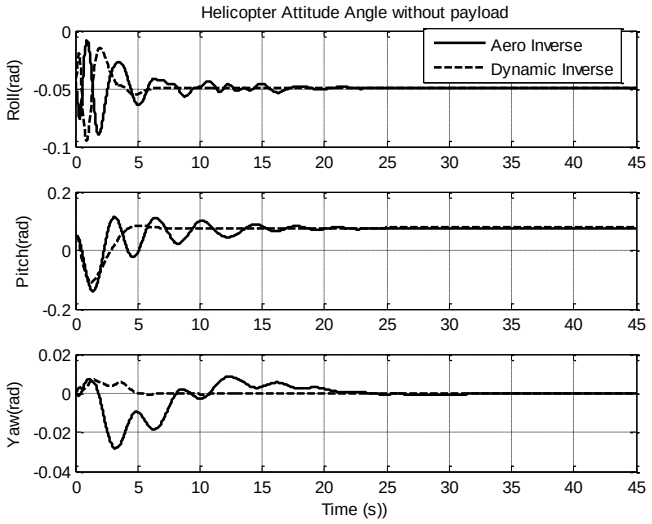

Figure 21 Attitude response without payload

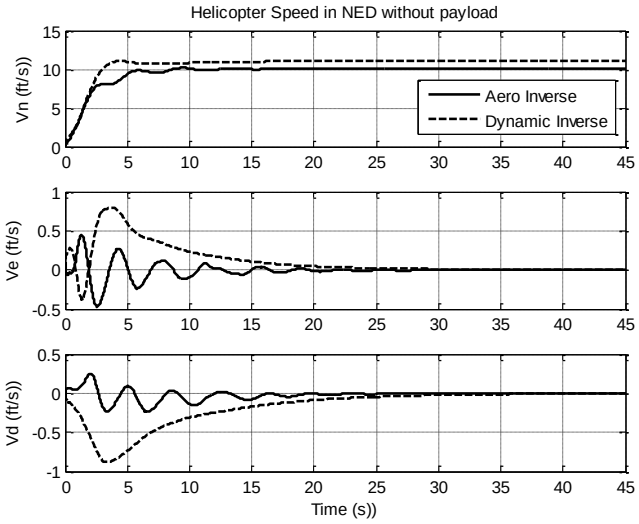

Figure 22 Velocity response without payload

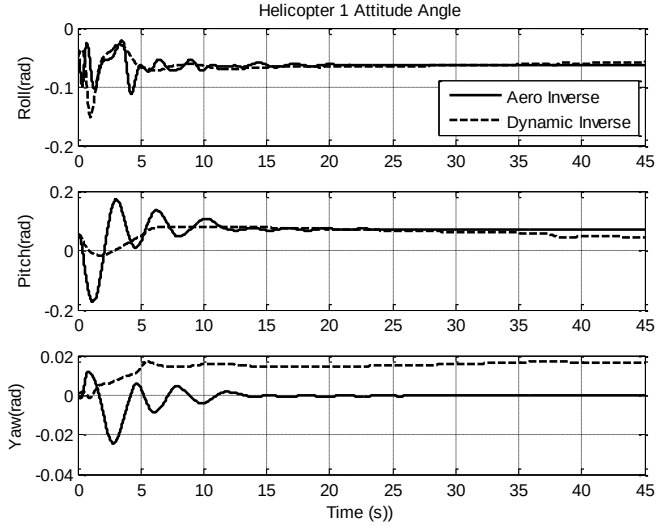

Figure 23 Attitude response of helicopter 1

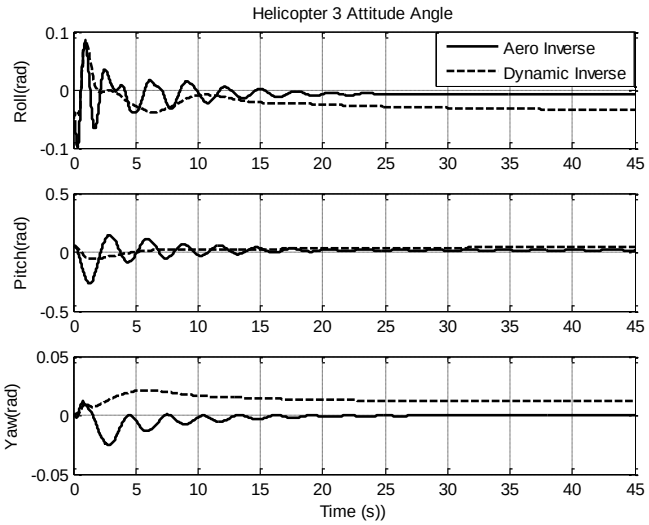

Figure 24 Attitude response of helicopter 3

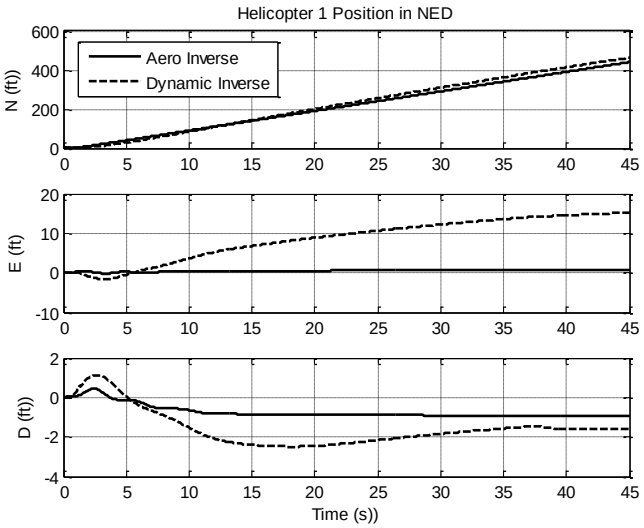

Figure 25 Position response of helicopter 1

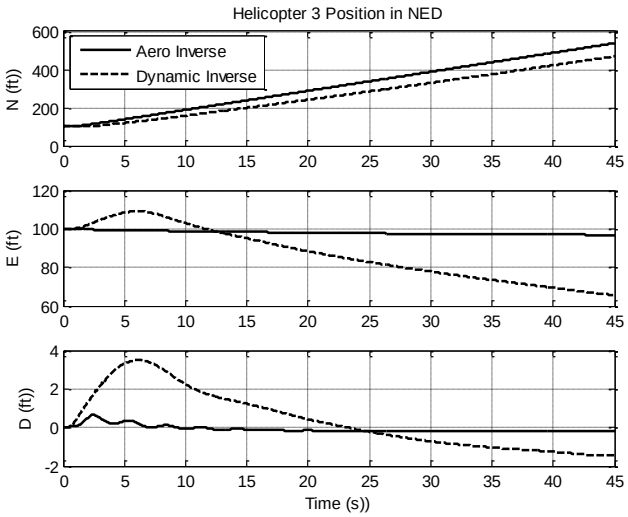

Figure 26 Position response of helicopter 3

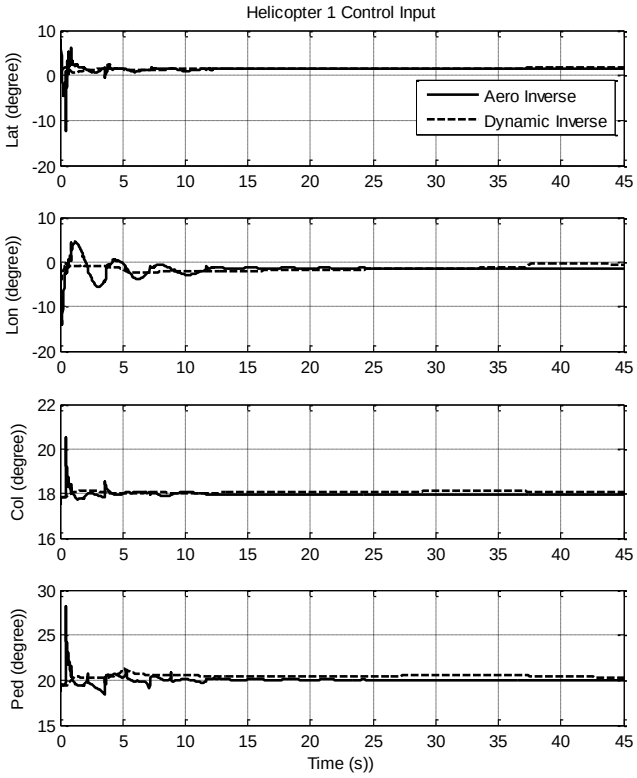

Figure 27 Control activity of helicopter 1

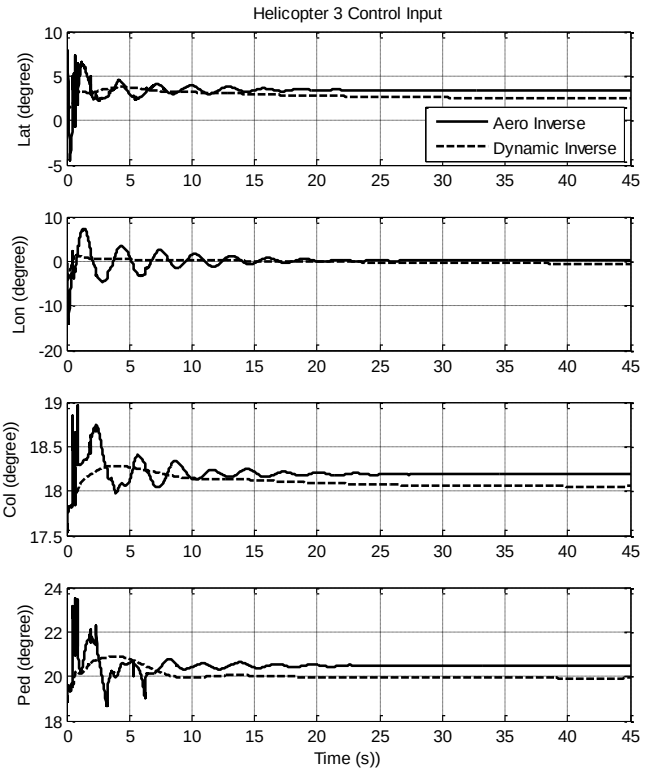

Figure 28 Control activity of helicopter 3

From the results, we can conclude that the overall performance of the proposed Aerodynamic Inverse scheme works better for the multi-lift system than that of the standard dynamic inversion controller. We still see the transient oscillations, but overall the Aerodynamic Inverse controller tracks the commanded trajectory more closely. This is critical for safe multi-lift flight. The main issue of the dynamic inversion controller is that it does not effectively account for the changing cable forces, which are significantly different for each helicopter in the formation. In the case of the dynamic inverse controller, the forward aircraft (H2 and H3) experience a drag force form the cable that causes them to lag behind the forward speed command, while the rear aircraft accurately track the command. Meanwhile, aircraft on both sides of the formation are pulled towards the center, with helicopters 1 and 2 drifting East, and helicopters 3 and 4 drifting West. The overall result is that the aircraft come closer to one another, presenting a hazardous situation.

The relative positions of each helicopter versus time are shown in Figures 29 and 30 for the dynamic inverse controller and the aerodynamic inverse controller respectively, where time is plotted on the vertical axis. The dynamic inverse controller is showing that the aircraft are likely to collide after a period of time, whereas the aerodynamic inverse controller is showing very good performance, with stable safe separation throughout the maneuver. The most likely reason for the poor performance of the dynamic inverse is lack of explicit knowledge of the cable loads in the inverse model. The dynamic inverse controller performance degrades further with heavier loads, and thus multi-lift simulations with this controller could only be tested for a relatively light payload of 3000 lbs.

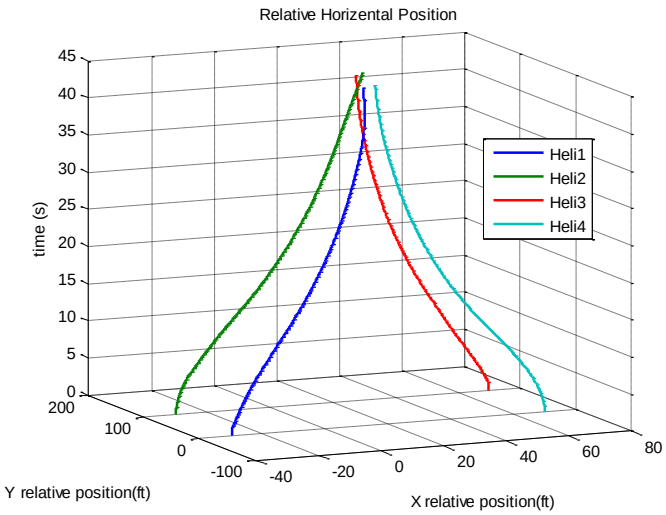

Figure 29 Helicopter relative positions with dynamic inverse controller

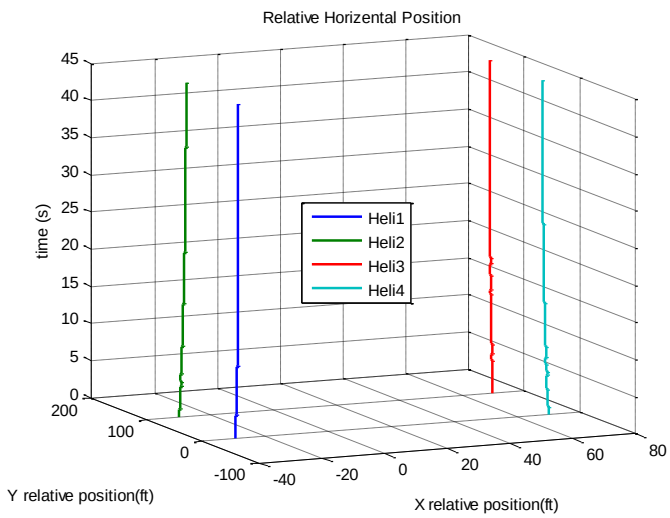

Figure 30 Helicopter relative positions with aerodynamic inverse controller

Now, in order to evaluate the performance of the aerodynamic inverse controller, we simulate a more complex maneuver to reposition a large external payload weighing 30,000 lbs. The desired ground track of the payload is shown in Figure 31. Synchronized trajectory commands are used for each helicopter to achieve the maneuver. The helicopters start in hover, climbs 50 ft at a rate of 10 ft/sec, then proceed along the path shown in Figure 31 at a forward ground speed of 10 ft/sec. The aircraft perform two 90° turns. The first turn is performed at a rate of 6 deg/sec to the right, and the second turn is performed at rate 10 deg/sec to the left.

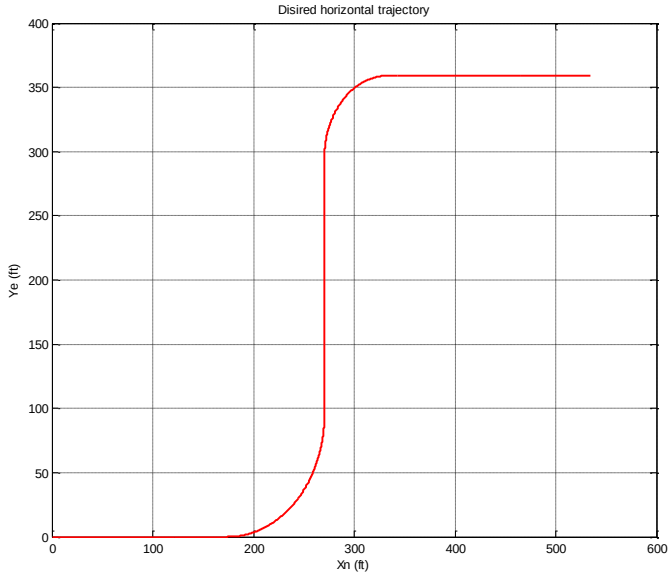

Figure 31 Desired trajectory for multi-lift maneuver

The results of the simulations for the multi-lift maneuver using the aerodynamic inverse controller are shown in Figures 32 to 34. Figure 32 shows the three-dimensional trajectory of each helicopter and the payload. Figure 33 shows relative position of each helicopter in the formation. There is some tendency for the helicopter to move closer to together, but they still maintain safe separation throughout. It should be noted that *no integrated position hold is currently included in the controller*, and each aircraft is only tracking a velocity command. The addition of a position hold function could be used to correct the drifting tendency.

Figure 34 shows the helicopter attitudes during the maneuver. The figure shows that while all helicopters are following similar trajectory, they must be experiencing significantly different loads from the external payload, as evidenced by the different attitudes during portions of the maneuver, especially after the first turn.

CONCLUSIONS

A generic simulation tool for dynamic modeling of helicopter multi-lift systems is presented. The simulation tool is implemented in the MATLAB / SIMULINK environment in a modular fashion so that it could readily be adapted to different multi-lift helicopter / payload configurations. Connecting cables are modeled as elastic elements, and a simple aerodynamic model of the payload is used. A simulation of a four helicopter / single payload multi-lift system is implemented. Initial trim solutions show reasonable behavior of the open-loop dynamic model.

A novel, non-linear control design is developed using the concept of an "aerodynamic inverse" method, where the controls are calculated to track a desired trajectory using an inversion of a simplified aerodynamic model and equations of motions. The inversion results in a compensated plant that behaves like a decoupled linear system, as done with control methods that use feedback linearization. Simple PID loops were then designed to track desired ground velocity, altitude, and heading. An advantage of the control scheme is that the measured cable force vector can be used explicitly in the control calculation to better reject disturbances due to the external load.

The controller was tested in closed-loop simulations and compared to a standard linear dynamic inverse controller. Simulation results showed that the aerodynamic inverse controller outperformed the dynamic inverse controller for simple multi-lift maneuvers with a light payload, whereas the standard dynamic controller could not provide safe separation. The aerodynamic inverse scheme was then tested for a heavy payload and a more complex multi-lift maneuver and showed good performance.

The following conclusions can be made from the results of these analyses:

1. The dynamic model shows the expected changes in trim state due to the external load, which varies according to the helicopter's location in the formation.

2. Linearization of the dynamic model showed significant change in eigenvalues, and therefore stability

characteristics of each helicopter due to the external load.

3. Each helicopter's trim, stability characteristics, and response characteristics will obviously change with weight of slung load, formation, and flight condition. This presents difficulties in coordinated control.

4. The aerodynamic inverse control scheme presented in the paper outperformed the classic dynamic inverse controller. However, it is possible that if a standard dynamic inverse could make use of measure cable forces it could achieve similar performance.

5. Whatever the underlying control scheme, the results indicate that the use of measured cable forces and moments can provide clear advantages in flight control performance, and can aid in the implementation of coordinated control for multi-lift.

.

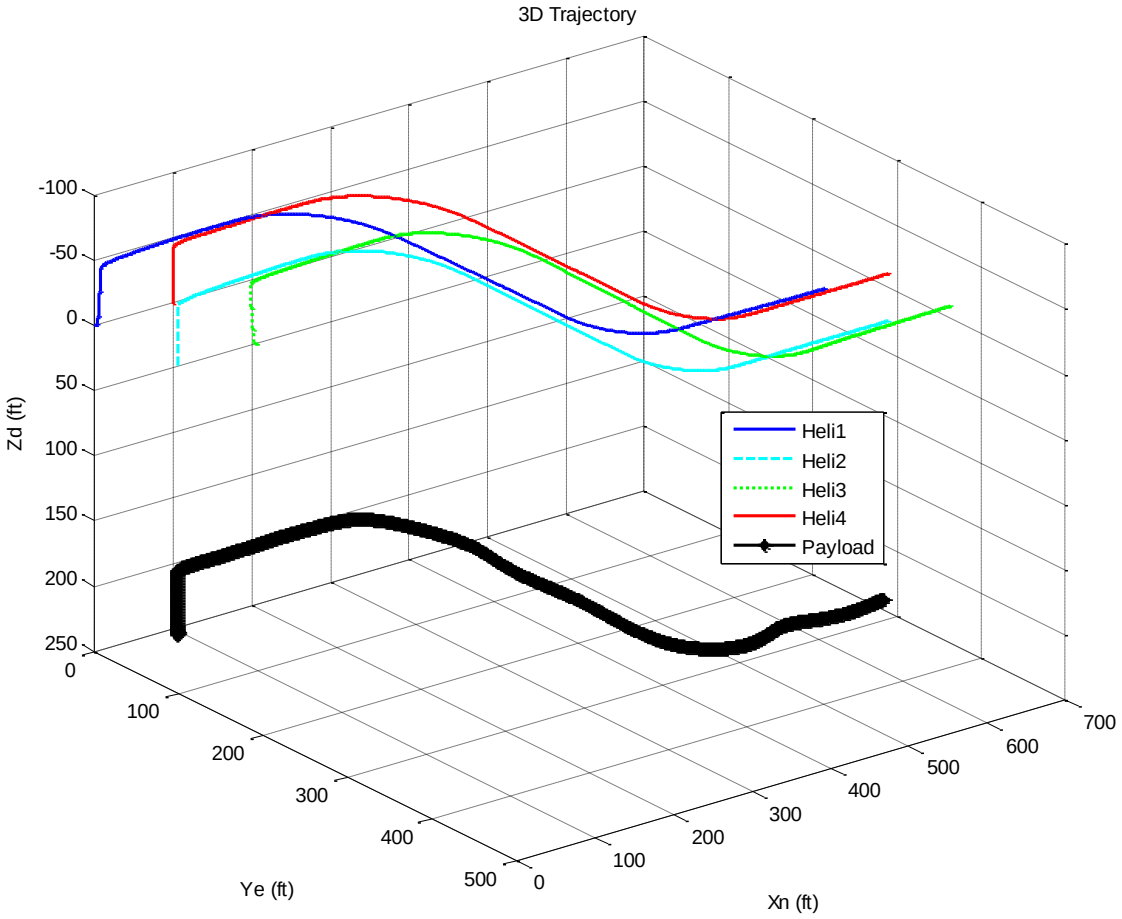

Figure 32 Helicopter and payload three-dimensional trajectories

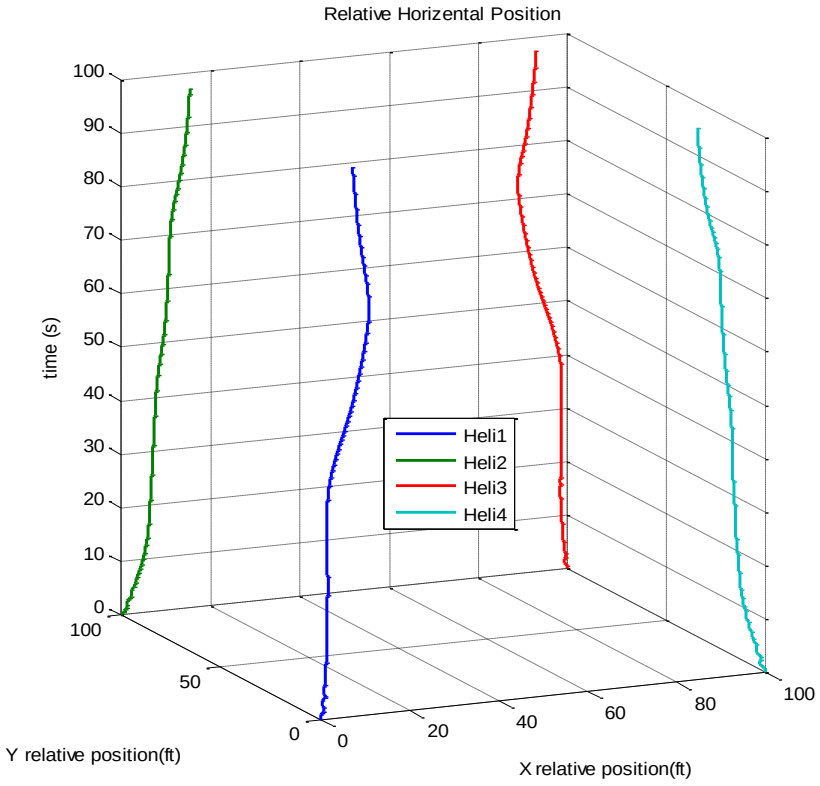

Figure 33 Relative positions during multi-lift maneuver simulation

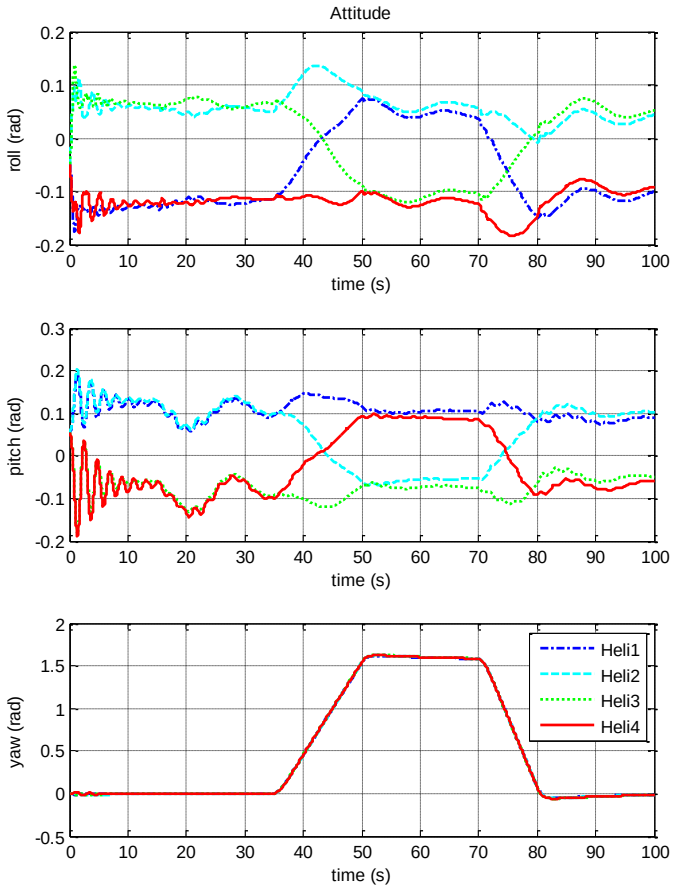

Figure 34 Helicopter attitudes during multi-lift maneuver simulation

ACKNOWLEDGMENTS

This research is partially funded by the Government under Agreement No. W911W6-11-2-0011. The U.S. Government is authorized to reproduce and distribute reprints notwithstanding any copyright notation thereon.

The views and conclusions contained in this document are those of the authors and should not be interpreted as representing the official policies, either expressed or implied, of the U.S. Government.

REFERENCES

[1] Lucassen, L. and Sterk, F. "Dynamic stability analysis of a hovering helicopter with a sling load," *Journal of the American Helicopter Society*, 1965 10(2): 6-12.

[2] Lusardi, J.A, Blanken, C.L., Braddom, S.R., et. al., "Development of External Load Handling Qualities Criteria," Proceedings of the American Helicopter Society 66th Annual Forum, Phoenix, AZ, May 11-13, 2010.

[3] Arthur W. G, "Preliminary Slung Load Investigation on the NRC Bell 412 Advanced Systems Research Aircraft," *Journal of the American Helicopter Society*, 2001 46(2):161-165.

[4] Briczinski, S.J., and Karas, G.R., "Criteria for Externally Suspended Helicopter Loads," USAAMRDL TR 71-61, November 1971.

[5] Mittal, M. and Prasad, J.V.R., "Three-Dimensional Modeling and Control of a Twin-Lift Helicopter System," *Journal of Guidance, Control, and Dynamics*, 1993, 16(1): 86~95.

[6] Mittal, M., Prasad, J. V. R., and Schrage, D. P., "Comparison of Stability and Control Characteristics of Two Twin-Lift Helicopter Configurations," *Journal of Nonlinear Dynamics*, 1992, 3(3): 199-223.

[7] Curtiss, H. C., and Warburton, F. W., "Stability and Control of the Twin Lift Helicopter System," *Journal of the American Helicopter Society*, 1985, 30(2):14-23.

[8] Maza I., Kondak K., Bernard M., Multi-UAV "Cooperation and Control for Load Transportation and Deployment," *Journal of Intelligent & Robotic Systems*, 2010 57(1):417–449.

[9] Cicolani. L.S., and Kanning G., "General Equilibrium Characteristics of a Dual-Lift Helicopter System," NASA/ TP-2615, 1986.

[10] Cicolani, L. S.; and Kanning, G, "Equations of Motion of Slung Load Systems with Results for Dual Lift," NASA TM-102246, Feb. 1990.

[11] Cicolani, L. S., and Kanning, G., "Equations of Motion of Slung Load Systems, Including Multi-Lift Systems," NASA TM 1038798, Sept. 1991.

[12] Morten B., Jan D. B., Anders C., "Modeling of Generic Slung Load System," *Journal Of Guidance, Control, And Dynamics* 2009 32(2):573-585.

[13] Sahasrabudhe, V., et al "Balancing CH-53K Handling Qualities and Stability Margin Requirements in the Presence of Heavy External Loads," Proceedings of the 63rd American Helicopter Society Annual Forum, Virginia Beach, VA, May 1-3, 2007.

[14] Hess, R. A., and Tran, P. M., "Pilot/Vehicle Analysis of a Twin-Lift Helicopter Configuration in Hover," *Journal of Guidance, Control, and Dynamics*, 1988, 11(5): 465-472.

[15] Prasad, J. V. R., Schrage, D. P., and Mittal, M., "Comparison of Nonlinear Controllers for Twin-Lift Configurations," Proceedings of the AIAA Guidance, Navigation, and Control Conference, Boston, Mass., August 1989: 1350-1357.

[16] Rodriguez, A. A., and Athans, M., "Multivariable Control of a Twin Lift Helicopter System using the LQG/LTR Design Methodology," Proceedings of the 1986 American Control Conference, June 1986: 1325-1332.

[17] Menon, P.K., Prasad, J.V.R, Schrage, D.P., "Nonlinear Control of a Twin-Lift Helicopter Configuration," *Journal of Guidance Control and Dynamics*, 1991, 14(6): 1287 – 1293.

[18] Mittal, M; Prasad, J.V.R; Schrage, D.P, "Nonlinear adaptive control of a twin lift helicopter system," *IEEE Control Systems*, 1991, 11(3): 39 – 45

[19] Prasad, J.V.R, Mittal, M., Schrage, D.P., "Control of a Twin Lift Helicopter System using Nonlinear State Feedback," *Journal of the American Helicopter Society*, 1991, 36(4): 57 - 65

[20] Meyer, G., Su, R., and Hunt, L. R., "Application of Nonlinear Transformations to Automatic Flight Control," *Automatica*, 1984, 20(1): 103-107.

[21] Glenn Lagace, "A Generalized Sling Load Model for the V-22 FFS," Proceedings of the American Helicopter Society 64th Annual Forum, Montréal, Canada, April 29 – May 1, 2008.

[22] Howlett, J., "UH-60A BLACK HAWK Engineering Simulation Program: Volume I – Mathematical Model", NASA-CR-166309, 1981.

[23] Gareth D. Padfield, *Helicopter Flight Dynamics: The Theory and Application of Flying qualities and Simulation Modeling*, Washington DC: AIAA Inc., 1996.

[24] Stevens, B.L., Lewis, F.L., *Aircraft Control and Simulation*, 2nd Ed., Wiley-Interscience, 2003.